Available online at www.sciencedirect.com
SCIENCE DIRECT®
Journal of Computational and Applied Mathematics 167 (2004) 91–134
JOURNAL OF COMPUTATIONAL AND APPLIED MATHEMATICS
www.elsevier.com/locate/cam

A geometric optics method for high-frequency electromagnetic fields computations near fold caustics—Part II. The energy

J.-D. Benamou*, O. Lafitte, I. Solliec, R. Sentis

INRIA, B.P. 105, F-78153 Le Chesnay Cedex, France

Received 20 November 2002; received in revised form 30 July 2003

Abstract

We present the computation of the amplitudes needed to evaluate the energy deposited by the laser wave in a plasma when a fold caustic forms. We first recall the Eulerian method designed in Benamou et al. (J. Comput. Appl. Math. 156 (2003) 93) to compute the caustic location and the phases associated to the two ray branches on its illuminated side. We then turn to the computation of the amplitudes needed to evaluate the energy. We use the classical geometrical form of the amplitudes to avoid the blow up problem at the caustic. As our proposed method is Eulerian we have to consider transport equations for these geometrical quantities where the advection field depends on the ray flow. The associated vector field structurally vanishes like the square root of the distance to the caustic when approaching the caustic. This introduces an additional difficulty as traditional finite difference scheme do not retain their accuracy for such advection fields. We propose a new scheme which remains of order 1 at the caustic and present a partial theoretical analysis as well as a numerical validation. We also test the capability of our Eulerian geometrical algorithm to produce numerical solution of the Helmholtz equation and attempt to check their frequency asymptotic accuracy.

Keywords: Hamilton–Jacobi; Hamiltonian system; Ray tracing; Viscosity solution; Upwind scheme; Geometric optics; Wave equation; Laser; Plasma; Electromagnetism; Transport equation

1. Introduction

This paper is the second and last part (the first part is [3]) presenting a Eulerian numerical method for the simulation of the propagation of a laser wave in a material medium.

The electromagnetic field A is the solution of the following frequency wave equation (see [8])

$$\nabla \cdot (\nabla A) + k_0^2 n^2 A + \mathrm{i}\nu k_0 A = 0. \tag{1}$$

* Corresponding author.
E-mail address: jean-david.benamou@inria.fr (J.-D. Benamou).

0377-0427/$ - see front matter © 2003 Published by Elsevier B.V.
doi:10.1016/j.cam.2003.09.046

The space variable X belongs to $\mathbb{R}^d$ ($d = 2$ in the sequel), ∇ is the gradient operator in $\mathbb{R}^d$, k_0 is the wave number of the laser wave in the vacuum, $n = n(X)$ is a strict positive function which corresponds to the refractive index of the medium and v a positive parameter characterizing the absorption coefficient of the laser energy by the material. The system is subject to an incident plane wave

$$A_{\text{inc}} = A_0 \exp(\mathrm{i}k_0 X(\cos\alpha, \sin\alpha)), \tag{2}$$

where α is the angle of incidence. Generally, one requires the index n to be constant when $|X| \to +\infty$ and the scattered field $A_{\text{scat}} = A - A_{\text{inc}}$ satisfies (in polar coordinates) the radiation boundary conditions at infinity:

$$\lim_{R\to\infty} \int_{S_R} \left| \frac{\partial}{\partial r} A_{\text{scat}} - \mathrm{i}k_0 A_{\text{scat}} \right|^2 \mathrm{d}\sigma = 0, \tag{3}$$

where S_R the sphere centered at 0 with radius R.

As in [3], a WKB technique is used (see, for example, [7]). In its simplest form the oscillatory unknown A is approximated by

$$A \simeq a\mathrm{e}^{\mathrm{i}k_0\phi}. \tag{4}$$

An asymptotic expansion of Eq. (1) shows that the phase ϕ satisfies the Eikonal equation

$$|\nabla\phi|^2 = n^2 \tag{5}$$

and the amplitude a is a solution to

$$va + 2\nabla a\nabla\phi + a\nabla\cdot(\nabla\phi) = 0. \tag{6}$$

The physical quantity $E = |a|^2$ which represents the laser energy satisfies

$$vE + \nabla\cdot(E\nabla\phi) = 0. \tag{7}$$

Both geometrical optics unknowns ϕ and a have slow variations compared to A and are cheaper to approximate and compute in terms of computational cost. The WKB approximation often is the only affordable way to simulate high-frequency wave propagation phenomena.

It is, however, well known that the single phase ansatz (4) is not correct in the vicinity of caustics for two related reasons: first, the rays which are the integral curves of the gradient of the phase $\nabla\phi$ and along which ϕ is defined cross and define a multi-valued phase function. Second, the same rays are the characteristics of the conservation law (7). Near the caustic neighboring rays cross and the Laplacian of the phase $\nabla.(\nabla\phi)$ is singular at the caustic. Eventually, the energy E computed by means of the WKB approximation becomes infinite.

The appropriate generalization of (4) is the Maslov theory of global oscillatory functions, which can be presented along the lines of the theory of Fourier integral operators of Hörmander [6]. A presentation of the application of this theory to the Helmholtz equation can be found in [7]. We will not use this theory but instead focus on a simple prototype example (already used in [3]) which can be solved analytically. In particular we show how the solution of (1) is linked to the notion of multi-valued solution of (5)–(6): Let us consider a 2D half-space problem $\{X = (z,x) \in \mathbb{R}^2 \,|\, x > 0\}$

which will simplify into a 1D problem as we assume the medium to be characterized by a simple index

$$n^2(z,x) = \begin{cases} 1 & \text{for } x < 0, \\ 1-x & \text{for } x \in [0, 1-\varepsilon], \\ \varepsilon & \text{for } x > 1-\varepsilon, \end{cases} \tag{8}$$

where we assume $\cos^2\alpha < 1-\varepsilon$ and $\varepsilon > 0$ is a small parameter.

The incoming wave determines the boundary condition data at $x=0$, and since n does not depend on z we can seek a solution of the form $A(z,x) = u(x)\exp(\mathrm{i}k_0 z \sin\alpha)$. Eq. (1) then simplifies to

$$\begin{aligned} &u''(x) + k_0^2 x_c u(x) + \mathrm{i}k_0 v u = 0 \quad \text{for } x < 0, \\ &u''(x) + k_0^2 (x_c - x) u(x) + \mathrm{i}k_0 v u = 0 \quad \text{for } x \in [0, 1-\varepsilon], \\ &u''(x) + k_0^2 (x_c - (1-\varepsilon)) u(x) + \mathrm{i}k_0 v u = 0 \quad \text{for } x > 1-\varepsilon, \end{aligned} \tag{9}$$

where $x_c = \cos^2\alpha$. The solution is given in the central zone as a linear combination of the airy Ai and airy of the second kind Bi functions [1].

Index (8) is not constant as $|X| \to +\infty$ and we are not aware of rigorous radiation boundary conditions in this case. It does however remain constant when $|x| \to +\infty$. We therefore complement Eq. (9) with 1D radiation boundary condition on $u_{\text{scat}} = u - u_{\text{inc}}$:

$$\begin{aligned} &\lim_{x\to+\infty} x \left(\frac{\partial}{\partial x} u_{\text{scat}} - \mathrm{i}k_0 \sqrt{x_c - (1-\varepsilon)}\, u_{\text{scat}} \right) = 0, \\ &\lim_{x\to-\infty} x \left(\frac{\partial}{\partial x} u_{\text{scat}} + \mathrm{i}k_0 \cos\alpha\, u_{\text{scat}} \right) = 0. \end{aligned} \tag{10}$$

Now, as the Bi function exponentially blows up with k_0 for $1 > x > x_c$ and as u is bounded, a tedious calculation shows that the Bi contribution is damped and an asymptotic approximation of u is given by

$$u(x) - Ck_0^{1/6} \mathrm{Ai}(-k_0^{2/3}((x_c - x) + \mathrm{i}v k_0^{-1})) = \mathrm{O}(k_0^{-\infty}) \tag{11}$$

the coefficient $k_0^{1/6}$ standing here for normalization purposes.

For $x - x_c < -\theta_0 < 0$, as $k_0 \to +\infty$, we get, using the classical asymptotic expansion of the Airy function [1] that

$$u(x) - \left\{ \frac{C}{2\sqrt{\pi}} \left(\frac{\mathrm{e}^{-\mathrm{i}\pi/4}}{(x_c - x)^{1/4}} \exp(\mathrm{i}k_0\zeta) + \frac{\mathrm{e}^{+\mathrm{i}\pi/4}}{(x_c - x)^{1/4}} \exp(-\mathrm{i}k_0\zeta) \right) \right\} \simeq \mathrm{O}(k_0^{-1}),$$

where

$$\zeta = \tfrac{2}{3}(x_c - x + \mathrm{i}v k_0^{-1})^{3/2}$$

that is to say

$$u(x) \simeq a^- \mathrm{e}^{\mathrm{i}\pi/4} \exp(-\mathrm{i}k_0\xi) + a^+ \mathrm{e}^{-\mathrm{i}\pi/4} \exp(\mathrm{i}k_0\xi) + \mathrm{O}(k_0^{-1}), \tag{12}$$

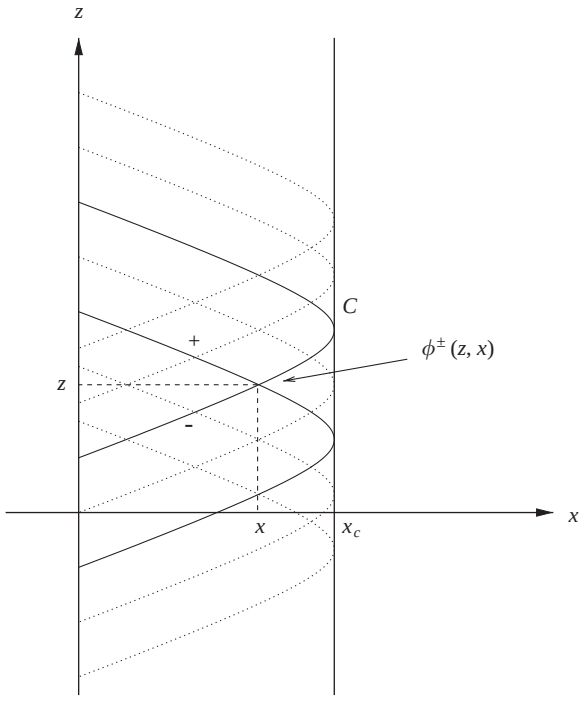

Fig. 1. The toy problem.

where $\xi = \frac{2}{3}(x_c - x)^{3/2}$ and

$$a^-(x) = \frac{C}{2\sqrt{\pi}} \frac{1}{(x_c - x)^{1/4}} e^{v\sqrt{x_c - x}}, \quad a^+(x) = \frac{C}{2\sqrt{\pi}} \frac{1}{(x_c - x)^{1/4}} e^{-v\sqrt{x_c - x}}. \tag{13}$$

Then we get the following approximation for the potential $A = u \exp(iz \sin\alpha)$:

$$A(z,x) - \{a^- e^{i\pi/4} \exp(ik_0\phi^-) + a^+ e^{-i\pi/4} \exp(ik_0\phi^+)\} \simeq O(k_0^{-1}) \tag{14}$$

with

$$\phi^{\pm}(z,x) = z \sin\alpha \pm \tfrac{2}{3}(x_c - x)^{3/2} + C. \tag{15}$$

In [3], we show that the rays of geometrical optics for this simplified toy problem produce a fold straight caustic curve $x = x_c$ (see Fig. 1) and predicts the amplitudes and phases (13)–(15). Each point on the illuminated side ($x < x_c$) of the caustic is reached by two rays which are labeled $-$ and $+$. The $-$ part of the rays propagate onto the caustic and is called direct while the $+$ part is the return portion of the rays after passing the caustic. Formula (14) means that at high frequency, A is the sum of two WKB ansatz formed by the $\pm$ branches. The $e^{\pm i\pi/4}$ terms represent the known $\pi/2$ phase shift across caustics according to Maslov theory. In Fig. 2, we have plotted in the case $v = 0$ both the exact solution A (plain line) and its WKB approximation (stars) (only in the last wavelength is a difference to be seen, the approximation blows at the caustic). A valid approximation of A near the caustic in the spirit of [10] is proposed in [9].

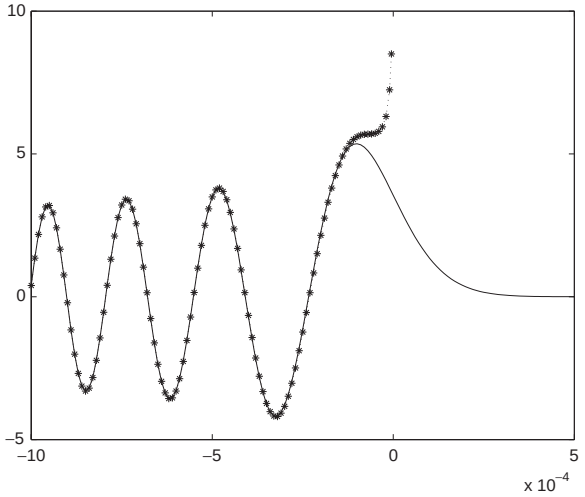

Fig. 2. The Airy function and its approximation.

From the application point of view an important physical quantity is the absorbed laser energy $\int_D |A|^2 \, \mathrm{d}X$ on a fixed domain D. One can readily check from (12) for $x < x_c$ that

$$|A|^2 = (|a^+|^2 + |a^-|^2) - 2a^+a^- \sin(2k_0\zeta) + \mathrm{O}(k_0^{-1}).$$

Recall that this approximation holds asymptotically in k_0 and therefore only the stationary points of ζ will contribute to the integral of the last term, actually only the caustic point. When the domain D is a strip $[x_1, x_2] \times [z_1, z_2]$ which does not contain the caustic $x = x_c$, we get by the Lebesgue lemma

$$\int_D |A|^2 \, \mathrm{d}X = \int_D (|a^+|^2 + |a^-|^2) \, \mathrm{d}X + \mathrm{O}(k_0^{-1/3}). \tag{16}$$

The integral on the right-hand side is the geometric optics approximation of the energy on the left-hand side. In our affine index of refraction case this integral is convergent for $x_2 = x_c$ and we show in Appendix A.1 that relation (16) remains true.

The numerical method presented in [3] and in this paper is designed to work for *general index of refraction* $n(z,x)$ *under the constraint that it produces a fold caustic*. In this case the asymptotic solution generically is of form (14). The phases $\phi^\pm$ and the amplitudes $a^\pm$ can generally only be computed numerically, the classical method being ray tracing. In [3], we proposed a Eulerian method for the computation of $\phi^\pm$. In this paper, we focus on the specific difficulties linked to the computation of the amplitudes or more precisely of the square of the amplitudes $E^\pm = |a^\pm|^2$. Owing to the singularity of the phase coefficients at the caustic neither (6) for $a^\pm$ nor (7) for $E^\pm$ are used in practice. Instead we use the conservative properties of Eq. (7) to establish the following representation for the energies:

$$E^\pm = \frac{Z^\pm}{|\Theta^\pm| \partial_z \phi^\pm}, \tag{17}$$

where $\Theta^\pm$ represents the oriented volume of an infinitesimal tube of rays (sometimes called "geometrical spreading") which vanishes at the caustic and Z is a function decaying along the rays at a

rate governed by v. These new unknowns are solutions of Eulerian transport equations and provide a robust evaluation across caustics.

The paper is organized as follows. We first summarize basic facts and results from our first paper [3] on the bi-valued phase $\phi^{\pm}$. We then derive in Section 3 the equations we will use to compute the amplitudes and numerically evaluate formula (16). Section 4 details more technical results on the modification of the computational domain and boundary/initial conditions. Section 5 explains the difficulty linked to the finite difference approximation of the transport equation near the caustic. We propose a first-order scheme and show numerical results. Finally Section 6 shows numerical results and presents a numerical validation of formulae (14) and (16) in the 1D case.

2. From the Lagrangian to the Eulerian modelization of the fold caustic

We give in the two following subsections, a necessary overview of the phase model presented in [3]. This presentation is slightly different and hopefully clearer than the one that can be found in [3].

In this section, and throughout the paper we use $d=2$ and $X=(z,x)$ is in $\mathbb{R}^2$ and $\nabla=(\partial_z,\partial_x)$. We believe that the content of this paper can be extended to treat fold caustic cases in three dimensions ($d=3$ and ∂_x is a gradient).

2.1. The Lagrangian model of the geometric optics

We start with an infinite device because it is in essence what our proposed Eulerian method can handle. The index $n(z,x)$ is constant ($=1$) in the half-plane $x<0$ where the incident plane wave (2) propagates freely. The important assumption on the physics of the problem in [3]—still required in this paper—was an a priori hypothesis on a qualitative behavior of the rays. In our (x,z) setting (see Fig. 4), we use the z-axis as a privileged direction of propagation. The rays start as straight lines making an angle α with the vertical axis in the $x<0$ half-plane (constant index of refraction), then they enter the $x>0$ area where the index has smooth variations such that rays "folds" and the locus of the fold is called the caustic. After turning back at the caustic the rays eventually exit the $x>0$ domain and revert to a straight line in the constant index part of the medium.

Remark that, from the geometrical point of view, nothing happens in the "shadow" zone behind the caustic. In the $x<0$ zone the incident plane wave obviously corresponds to the direct rays and we thus assume that the return rays can be associated to the scattered part of the solution. It therefore seems natural for return rays to satisfy some out-flow condition consistent with the radiation boundary condition.

The "fold caustic" assumption can be mathematically expressed by two conditions. First the ray curves can be parameterized by z and so is the caustic denoted by $x=x_c(z)$. Second, every point (x,z) on the illuminated side of the caustic is passed by two rays, the other side (the shadow zone) is not reached. They can be classified into two "branches": *direct* rays that reach the point before passing through the caustic and *return* rays that reach the point after.

We define the family of ray curves $\{y(z,z_0),\ z_0\in\mathbb{R},\ z>z_0\}$ (see Fig. 4) where z_0 indicates the first crossing position of the ray with the $x=0$ axis (Γ_{inc}). The rays are solutions, $\forall z_0$ and $\forall z>z_0$

of the 1D Hamiltonian system:

$$\begin{aligned} \dot{y}(z,z_0) &= H_p(z,y,p), \\ \dot{p}(z,z_0) &= -H_x(z,y,p), \\ \dot{\varphi}(z,z_0) &= p\cdot H_p(z,y,p) - H(z,y,p), \end{aligned} \tag{18}$$

where $H(z,x,p) = -\sqrt{n^2 - p^2}$. The dot stands for differentiation with respect to z, and H_x and H_p denote the derivatives of H with respect to x and p. We specify the initial conditions on the axis $x = 0$

$$\begin{aligned} y(z_0,z_0) &= 0, \\ p(z_0,z_0) &= \sin\alpha, \\ \varphi(z_0,z_0) &= \sin\alpha z_0. \end{aligned} \tag{19}$$

The initial conditions are derived from the incident plane wave condition (2) and all rays can be extended backwards by straight lines (they solve the same equation in the $x < 0$ zone).

2.2. The truncated and extended Lagrangian model

2.2.1. The truncated Lagrangian model

In practice our device is finite and the index n defined in a bounded interval. We can still assume the domain to be infinite in the $x < 0$ half-plane as the propagation is trivial there but we need also to bound the domain in the z direction. Let us set $]0,Z[$ as the range in z where the index is defined. There is no difficulties to stop the ray computations at $z = Z$ and truncate the domain there. Truncating at $z = 0$ is more problematic. Notice indeed that if we use initialization (19) but only for positive z_0. It generates different zones where the fold caustic hypothesis above does not necessarily applies. There is a first zone labeled (1) in Fig. 5 below the first ray shot from the origin $(0,0)$, represented in thick line, which is not covered by any rays. A second zone labeled (2) delimited by the direct part and return part of that same first ray is only reached by direct rays. We finally on the remaining part of the illuminated domain, labeled (3) on the figure where we get the usual "fold caustic" regime where every point is reached by a direct and a return ray.

2.2.2. The extended Lagrangian model

As already hinted, and extensively explained in [3], the truncation of the Lagrangian model is a source of difficulties when we want to switch to an Eulerian treatment. Indeed, both the direct and return part of the solution are sought for as coupled Eulerian solutions of evolution partial differential equations in z and the coupling cannot be avoided to compute the caustic. Initial conditions are therefore needed for both branches at $z = 0$.

In [3] we proposed initial conditions derived from a compatible stationary problem: the index is first extended in the $z < 0$ by setting $n(z,x) = n(0,x), \forall z < 0$. As the z dependence is suppressed, all rays issued from negative z_0 have the same behavior and the caustic is a straight line $x_c(z) = C_0$. It can be shown [10] that this "stationary" solution has a $C^{2,1}$ connection with the solution in the $z > 0$ domain (see Fig. 6). This extension process has two advantages. First we now have two branches everywhere in the physical domain, second the stationary solutions at $z = 0$ are easy to compute and can be used as initial data.

We can therefore truncate anew this extended model at $z = 0$ and set the initial conditions for the ray system on the x-axis (Fig. 7). Note that according to the "fold caustic" hypothesis each point $(z = 0, x_0)$ for $x_0 \in]-\infty, C_0[$ is reached by two rays of the extended model. We now have two families of rays curves now parameterized by x_0 instead of z_0 : $\{y_i(z, x_0), x_0 \in]-\infty, C_0[,\ z > 0\}$ for $i = 1, 2$ where $y_1(z, x_0)$, respectively, $y_2(z, x_0)$, are the rays issued from the direct, respectively return, rays crossing $z = 0$ at x_0. The rays of each family satisfy for $\forall z > 0$ of the same system (18) and the initial conditions now derive from truncating the extended model:

$$\begin{aligned} &y_i(0, x_0) = x_0, \\ &p_i(0, x_0) = p_{i,0}(x_0), \\ &\varphi_i(0, x_0) = \varphi_{i,0}(x_0), \end{aligned} \tag{20}$$

where $p_{1,0}$ and $\varphi_{1,0}$ are data of the problem, $p_{2,0}$ and $\varphi_{2,0}$ are by-products of the stationary problem in $z < 0$ and $p_i(., x_0)$ and $\varphi_i(., x_0)$ are the corresponding solutions of (18).

2.3. From Lagrangian to Eulerian

The rays of the y_2 family will always be return rays, they passed the caustic in the extension $x < 0$ of the domain; we will denote these rays y_2^+. This is not the case for the y_1 family in which the rays start as direct rays, pass the caustic and become return rays (Figs. 3–7). The direct part of a y_1 rays will be denoted y_1^- and the return part y_1^+. Mathematically, $\forall x_0$, there is a depth $z_c(x_0)$ such that

$$y_1(z_c(x_0), x_0) = x_c(z_c(x_0))$$

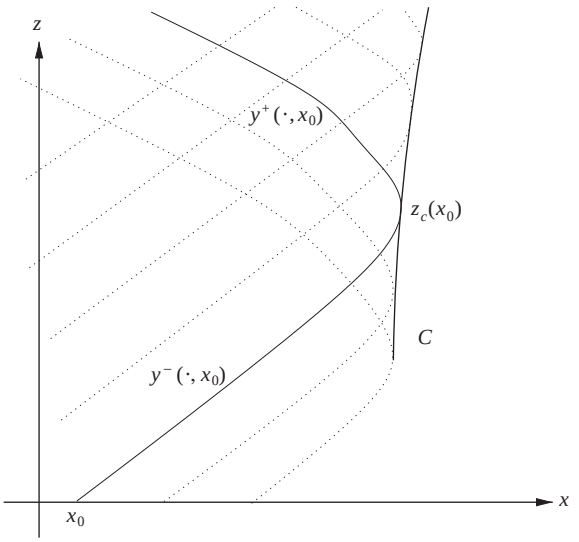

Fig. 3. The $y^{\pm}$ splitting.

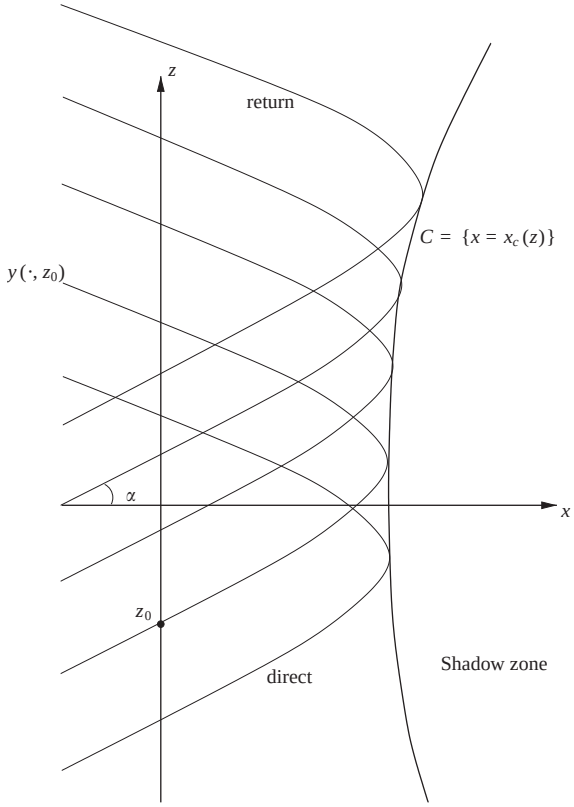

Fig. 4. The infinite model.

and then

$$y_1^-(z,x_0) = y_1(z,x_0) \quad \text{for } z \leqslant z_c(x_0),$$

$$y_1^+(z,x_0) = y_1(z,x_0) \quad \text{for } z \leqslant z_c(x_0).$$

We can now assert that every point $(z,x) \in]0,Z[\times]0,x_c(z)[$ is passed by two rays (Fig. 1): a direct ray which is necessarily a y_1^- rays and a return ray which is either a y_1^+ or a y_2^+ ray. Thus, for all x_0 the formulae

$$\phi^-(z, y_1^-(z,x_0)) = \varphi_1(z,x_0) \tag{21}$$

for the direct branch and

$$\phi^+(z, y_1^+(z,x_0)) = \varphi_1(z,x_0), \quad \phi^+(z, y_2^+(z,x_0)) = \varphi_2(z,x_0) \tag{22}$$

for the return branch, define two single valued Eulerian phase functions $\phi^+(z,x)$ and $\phi^-(z,x)$.

We recall the full Eulerian model for $\phi^\pm$ and associated initial and boundary conditions derived in [3]:

$$\partial_z \phi^\pm(z,x) + H(z,x,\partial_x \phi^\pm) = 0 \quad \text{for } (z,x) \in \mathbb{R}^+ \times [0,x_c(z)]. \tag{23}$$

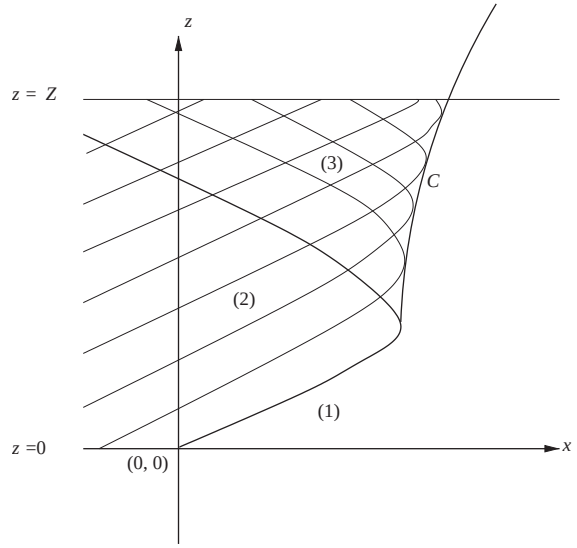

Fig. 5. The bounded model.

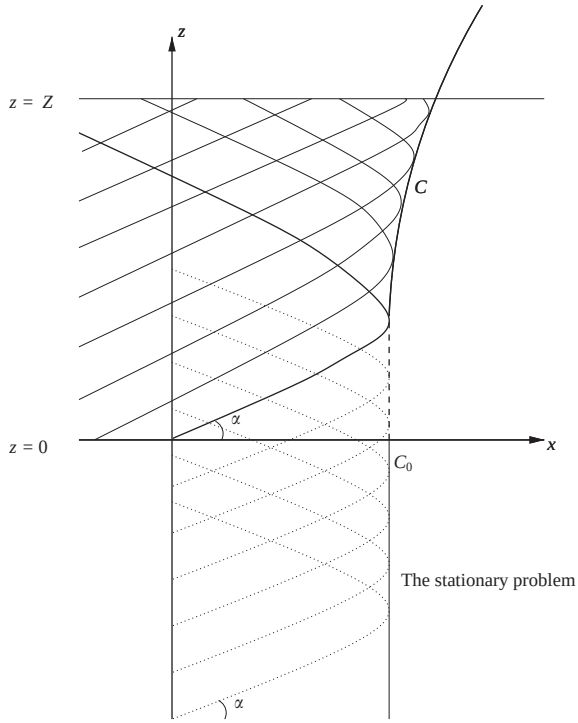

Fig. 6. Initialization by a stationary problem.

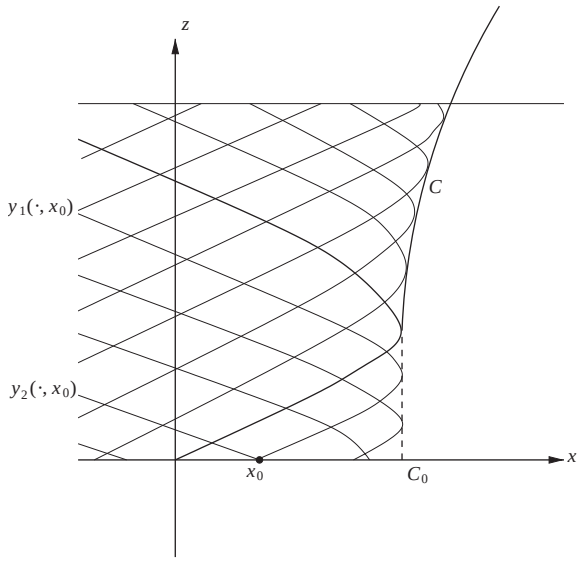

Fig. 7. The full bounded model.

We use an incoming boundary conditions on ϕ^-

$$\phi^-(z,0) = \phi_{\text{inc}}(z) \quad \text{for } z \geqslant 0. \tag{24}$$

Initial conditions are derived from a compatible stationary problem [3] (we return to this in Section 4.1).

The direct and return phases (and, as they satisfy the same equation, their gradient) match at the caustic

$$\phi^+(z, x_c(z)) = \phi^-(z, x_c(z)) \quad \text{for } z \geqslant 0 \tag{25}$$

and one can check that

$$\dot{x}_c(z) = H_p(z, x_c(z), p_c(z)), \qquad p_c(z) = \partial_x \phi^{\pm}(z, x_c(z)). \tag{26}$$

Both (26) and (23) are consequences of the identification formula

$$p(z, x_0) = \partial_x \phi(z, y(z, x_0)), \tag{27}$$

which holds for both families of rays or branches. We use this property to define the Eulerian flows:

$$\mathscr{V}^{\pm}(z,x) = H_p(z, x, \partial_x \phi^{\pm}(z,x)) = -\frac{\partial_x \phi^{\pm}(z,x)}{H(z, x, \partial_x \phi^{\pm}(z,x))} = \frac{\partial_x \phi^{\pm}(z,x)}{\partial_z \phi^{\pm}(z,x)}$$

corresponding to the Lagrangian flows, i.e., the first line of (18).

2.4. Eulerian–Lagrangian function correspondence

As already done for the bi-valued phase (21)–(22), we systematically define bi-valued Eulerian function from their Lagrangian counterparts. We consider a couple of Lagrangian functions $\mathbf{U}_1(z, x_0)$

and $\mathbf{U}_2(z,x_0)$ which are transported along the $y_{1,2}$ rays according to the ordinary differential equation

$$\partial_z \mathbf{U}_i = f(\mathbf{U}_i).$$

As in (21)–(22), we can define two Eulerian functions $U^{\pm}(z,x)$ by

$$U^-(z, y_1^-(z,x_0)) = \mathbf{U}_1(z,x_0), \quad U^+(z, y_i^+(z,x_0)) = \mathbf{U}_i(z,x_0), \quad i = 1,2, \ \forall x_0. \tag{28}$$

Remark. As rays y_1^+ and y_2^+ never cross we will in the sequel unambiguously note simply y^+ for the return rays and y^- for the direct rays (instead of y_1^-). They satisfy the ODEs

$$\dot{y}^{\pm}(z) = \mathscr{V}^{\pm}(z, y^{\pm}(z)).$$

The Eulerian functions satisfy the partial differential equations obtained by differentiating the above relations:

$$\partial_z U^{\pm} + \mathscr{V}^{\pm}(z,x)\partial_x U^{\pm} = f(U^{\pm}(z,x)). \tag{29}$$

Also, remark that branches necessarily match at the caustic

$$U^+(z, x_c(z)) = U^-(z, x_c(z)). \tag{30}$$

We already used this expression for phases (25) and will use it again to derive boundary conditions.

3. The energy/amplitude model

The aim of this subsection is explain how the energy densities $E^{\pm} = |a^{\pm}|^2$ used in formula (16) are evaluated. The classical method for the computation of the energy densities uses a Lagrangian formula obtained from the integration of (7) on a ray tube. We first detail this derivation leading to formula (17) and introduce geometrical spreading $\Theta^{\pm}$ and the auxiliary variables $Z^{\pm}$. We then give the Eulerian equations used to compute these new quantities. Finally we give an equivalent fully Eulerian derivation of the same equations.

3.1. The Lagrangian approach for $E^{\pm}$

We start by considering a tube around a reference ray $y^-(z,\bar{x}_0)$ in the direct part of the Lagrangian solution and will omit the $.^-$ notation for convenience. A ray tube is defined as $\Omega = \{(z, y(z,x_0)),\ z \in]z_0,z_1[,\ x_0 \in B(\bar{x}_0,\varepsilon)\}$ where $B(\bar{x}_0,\varepsilon)$ is the ball of radius ε and center $\bar{x}_0$, and z_0, z_1 are fixed (see Fig. 8). The integration of Eq. (7) on Ω gives (by Green's formula)

$$\int_{\{z=z_1\}\cap\partial\Omega} E(z_1,x)\nabla\phi(z_1,x)\cdot\vec{n}\,\mathrm{d}x = \int_{\{z=z_0\}\cap\partial\Omega} E(z_0,x)\nabla\phi(z_0,x)\cdot\vec{n}\,\mathrm{d}x + \int_{\Omega} vE(z,x)\,\mathrm{d}x\,\mathrm{d}z,$$

where $\vec{n}$ is the exterior normal to $\partial\Omega$. It is simply here $(\pm 1, 0)$ in the two terms above and then $\nabla\phi\cdot\vec{n} = \pm\partial_z\phi$. The remaining parts of $\partial\Omega$ are rays portions and their contribution is zero as $\nabla\phi$ is tangent to the rays by construction.

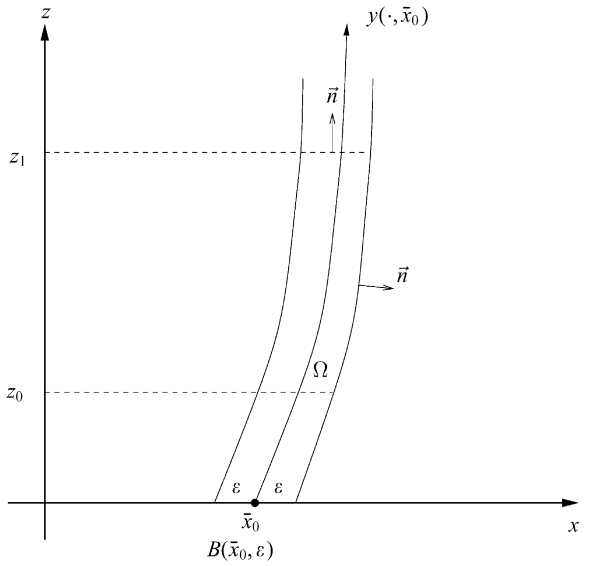

Fig. 8. A tube of rays.

We now change the integration variable $x \to x_0 = y^{-1}(z,x)$ (i.e., $x = y(z,x_0)$):

$$\int_{B(\bar{x}_0,\varepsilon)} E(z_1, y(z_1,x_0))\partial_z\phi(z_1, y(z_1,x_0))|\partial_{x_0} y(z_1,x_0)|\,\mathrm{d}x_0$$

$$= \int_{B(\bar{x}_0,\varepsilon)} E(z_0, y(z_0,x_0))\partial_z\phi(z_0,x_0)\,\mathrm{d}x_0$$

$$+ \int_{z_0}^{z_1}\int_{B(\bar{x}_0,\varepsilon)} vE(z, y(z,x_0))|\partial_{x_0} y(z,x_0)|\,\mathrm{d}x_0\,\mathrm{d}z$$

and obtain a formula for the energy—along every ray ($\forall x_0$) and for all $z \in]z_0, z_1[$—by letting ε go to 0

$$E(z, y(z,x_0))\partial_z\phi(z, y(z,x_0))|\partial_{x_0} y(z,x_0)|$$

$$= E(z_0,x_0)\partial_z\phi(z_0,x_0)|\partial_{x_0} y(z_0,x_0)| + \int_{z_0}^{z} vE(z, y(z,x_0))|\partial_{x_0} y(z_0,x_0)|\,\mathrm{d}z. \tag{31}$$

Let us assume for a while that $v = 0$. Then equation (31) simply states the well-known conservation property according to which $E \times (\partial_z\phi|\partial_{x_0} y|)$ is constant along rays. Indeed the oriented volume of an infinitesimal tube of rays reduces to $\partial_z\phi|\partial_{x_0} y|$ in the paraxial model.

Of course, formula (31) is meaningful as long as the ray tube does not collapse; we recall that we are in the direct part of the rays and $\partial_{x_0} y^-(z,x_0) \neq 0$. At caustic points, $\partial_{x_0} y^-(z,x_0)$ vanishes and (31) predicts an infinite energy density. To overcome the caustic difficulty we define a new function $Z^-(z,x)$:

$$Z^-(z, y^-(z,x_0)) = E^-(z, y^-(z,x_0))\partial_z\phi^-(z, y^-(z,x_0))|\partial_{x_0} y^-(z,x_0)|. \tag{32}$$

We find from (31) that $Z^-(z, y^-(z,x_0))$ satisfies the ODE

$$\partial_z\{Z^-(z, y^-(z,x_0))\} = -v\,\frac{Z^-(z, y^-(z,x_0))}{\partial_z\phi^-(z, y^-(z,x_0))},$$

$$Z^-(0,x_0) = E^-(0,x_0)\partial_z\phi^-(0,x_0) \tag{33}$$

(recall that $y(0,x_0) = x_0$). Thus, as we assumed $\partial_z\phi > 0$ (Section 2.1), Z^- remains bounded even at the caustic.

We now can repeat the above computations in the return part of the solution and in particular a Z^+ function can be defined that satisfies the ODE (33) after the caustic. Assuming that the following continuity condition on Z (proved in [11]) holds:

$$Z^+(z, y^+(z,x_c(z))) = Z^-(z, y^-(z,x_c(z))), \tag{34}$$

we obtain a uniformly valid formula (except at caustic points) for the energy density along a ray:

$$E^\pm(z, y^\pm(z,x_0)) = \frac{Z^\pm(z, y^\pm(z,x_0))}{\partial_z\phi^\pm(z, y^\pm(z,x_0))|\Theta^\pm(z, y^\pm(z,x_0))|}, \tag{35}$$

where

$$\Theta^\pm(z, y^\pm(z,x_0)) = \partial_{x_0} y^\pm(z,x_0).$$

In Eulerian coordinates we have the formulae

$$E^\pm = \frac{Z^\pm}{\Theta^\pm\partial_z\phi^\pm}\ (=|a^\pm|^2). \tag{36}$$

It is shown in [9] that for any bounded sub-domain D of $\{(z,x)\ \text{s.t.}\ x \leqslant x_c(z),\ z > 0\}$, we obtain

$$\int_D |A|^2\,\mathrm{d}X = \int_D \left(\frac{Z^-}{\Theta^-\partial_z\phi^-} + \frac{Z^+}{|\Theta^+|\partial_z\phi^+}\right)\mathrm{d}X + \mathrm{O}(k_0^{-1/3}) \tag{37}$$

generalizing (16).

3.2. Eulerian equations for Z and Θ

The Lagrangian ODE for $Z(z, y(z,x_0))$ (33) considered as a function of (z,x_0) is given in the previous section. Its solution is

$$Z(z, y(z,x_0)) = Z(0,x_0)\exp\left(-\int_0^z \frac{v}{\partial_z\phi(z, y(z,x_0))}\,\mathrm{d}z\right)$$

and illustrates the absorption effect of the v term in (7). As $\nabla_{z,x}\phi^+ = \nabla_{z,x}\phi^-$ at the caustic, this formula is correct even across the caustic (thanks to (34)). In particular when $v = 0$, Z is a constant and this constant is preserved both along the direct and return part of the rays.

We of course apply the Lagrangian to Eulerian transformation of Section 2.3 and find a set of two equations for $Z^\pm$:

$$\partial_z Z^\pm + \mathscr{V}^\pm\partial_x Z^\pm = -\frac{v}{\partial_z\phi^\pm)}\,Z^\pm \tag{38}$$

linked by $Z^-(z,x_c(z)) = Z^+(z,x_c(z))$ on the caustic (use (30)). A direct derivation of this equation can be found in Appendix A.4.

Geometrical spreading depends on the evaluation of $\partial_{x_0} y(z,x_0)$. In the ray tracing method, this is done through the linearization of the Hamiltonian system (18) with respect to x_0 (for both direct and return components)

$$\partial_z \begin{pmatrix} \partial_{x_0} y(z,x_0) \\ \partial_{x_0} p(z,x_0) \end{pmatrix} = \begin{pmatrix} H_{xp}(z,y,p) & H_{pp}(z,y,p) \\ -H_{xx}(z,y,p) & -H_{xp}(z,y,p) \end{pmatrix} \begin{pmatrix} \partial_{x_0} y(z,x_0) \\ \partial_{x_0} p(z,x_0) \end{pmatrix} \tag{39}$$

and initial conditions

$$\begin{pmatrix} \partial_{x_0} y(0,x_0) \\ \partial_{x_0} p(0,x_0) \end{pmatrix} = \begin{pmatrix} 1 \\ \partial^2_{x_0^2} \phi_0 \end{pmatrix}.$$

As for $\Theta^\pm$ we define $\Lambda^\pm(z,x)$ using the Lagrangian coordinates

$$\Lambda^\pm(z, y(z,x_0^\pm)) = \partial_{x_0} p(z,x_0^\pm).$$

We find (see Section 2.3) that they satisfy the Eulerian system of partial differential equation derived from (39) [2],

$$\begin{aligned} &\partial_z \begin{pmatrix} \Theta^\pm \\ \Lambda^\pm \end{pmatrix} + H_p(z,x,\nabla\phi)\partial_x \begin{pmatrix} \Theta^\pm \\ \Lambda^\pm \end{pmatrix} \\ &\quad = \begin{pmatrix} H_{xp}(z,x,\nabla\phi) & H_{pp}(z,x,\nabla\phi) \\ -H_{xx}(z,x,\nabla\phi) & -H_{xp}(z,x,\nabla\phi) \end{pmatrix} \begin{pmatrix} \Theta^\pm \\ \Lambda^\pm \end{pmatrix} \end{aligned} \tag{40}$$

with $\Lambda^-(z,x_c(z)) = \Lambda^+(z,x_c(z))$ and necessarily $\Theta^-(z,x_c(z)) = \Theta^+(z,x_c(z)) = 0$ on the caustic.

4. Computational domain, boundary and initial conditions

One key issue of the problem is the determination of the computational domain as well as Eulerian initial and boundary conditions. The domain is a strip bounded on the $x > 0$ side (should the laser come from the $x < 0$ side) by the caustic curve $x = x_c(z)$ and on the other side by the $x = 0$ axis (see any figure). The physics is indeed trivial in the $x < 0$ half-plane where the index is assumed to be constant. By definition the direct $(-)$ solution in this zone is associated to the incident plane wave $A_0 \exp(ik_0(z\sin\alpha + x\cos\alpha))$ while the return $(+)$ solution is expected to propagate freely away in the $x < 0$ direction because of the radiation boundary condition imposed on the scattered field. This is the input data we must build on to determine our boundary and initial conditions.

4.1. Boundary conditions

As already mentioned (Sections 3.2, 3.3), the boundary conditions on the caustic side all derive from formula (30). All quantities that are transported by the ray flow must match at the caustic, and in addition geometrical spreading is known to vanish there.

As in [3] all direct $(-)$ quantities are linked to the incident plane wave (2); its geometric interpretation forms a uniform set of rays at an angle α with the boundary $x=0$ (Fig. 6). It provides—the index of refraction is constant equal to one on the boundary—either a Neumann $\partial_x\phi^- = \cos\alpha$ or a Dirichlet $\phi^- = \phi_{\text{inc}} = z\sin\alpha$ boundary condition for the direct phase (see [3] for more details). We recall that $\{\Theta^-(z, y(z,x_0)), \Lambda^-(z, y(z,x_0))\} = \{\partial_{x_0} y(z,x_0), \partial_{x_0} p(z,x_0)\}$ where x_0 is the initial position of the tracked ray $y(z,x_0)$ on the x-axis. The resolution of (39) is trivial in the $x<0$ where the index of refraction is constant. The solution is constant and its trace on $x=0$ gives the boundary conditions

$$\Theta^-(z,0) = 1, \quad \Lambda^-(z,0) = 0.$$

The quantity Z^- is linked to the incoming amplitude A_0 through formula (36):

$$Z^- = E^-\Theta^-\partial_z\phi^- = |A_0|^2\Theta^-\partial_z\phi^-. \tag{41}$$

The incident wave models a laser beam of a given thickness that first propagates undisturbed in the $x<0$ zone, so Z will be zero everywhere on $x=0$ except on a given window $]z_0,z_1[$ where it simply is one. In practice we use a smoothed (depending on a parameter ε) characteristic function (see Fig. 16):

$$Z^-(z,0) = |\Xi^{\varepsilon}_{]z_0,z_1[}|^2\sin\alpha.$$

Like for phase functions, no boundary conditions on $x=0$ are needed for all return quantities Θ^+, Λ^+ and Z^+ as we assume (a feature of the fold caustic case) that the return flow goes out of our computational domain.

4.2. Initial conditions at $z=0$

As we already recalled (Section 2.2), the localization of the caustic curve depends on a model coupling both the direct and return phases with the caustic equation itself. We therefore need to provide initial Cauchy data for all (direct $-$ and return $+$) quantities.

We explained in [3] how to extend the solution to a pseudo-stationary bi-valued model in the $z<0$ zone (the index is only a priori given $\forall z \geqslant 0$) that reduces to an easily computable 1D problem. We then showed that it provides a noninterfering Cauchy data for system (23)—noninterfering here meaning that the stationary solution and the actual solution associated to incident plane wave do not overlap and continuously connect. It defines in particular an initial caustic point $x_c(0)=C_0$, see Fig. 6 and [3] for details.

The same strategy applies to the transported quantities above and the initial Cauchy data are given by the solutions $(\Theta_0^{\pm}, \Lambda_0^{\pm})$ of the stationary equations (both for $\pm$ branches):

$$H_p(0,x,\nabla\phi^{\pm}(0,x))\cdot\partial_x\begin{pmatrix}\Theta_0^{\pm}\\ \Lambda_0^{\pm}\end{pmatrix} = \begin{pmatrix} H_{xp}(0,x,\nabla\phi^{\pm}(0,x)) & H_{pp}(0,x,\nabla\phi^{\pm}(0,x))\\ -H_{xx}(0,x,\nabla\phi^{\pm}(0,x)) & -H_{xp}(0,x,\nabla\phi^{\pm}(0,x))\end{pmatrix}\begin{pmatrix}\Theta_0^{\pm}\\ \Lambda_0^{\pm}\end{pmatrix}.$$

We know the exact solution to these equations: up to the multiplicative constant C:

$$\Theta_0^{\pm}(x) = \mp 2C\sqrt{n^2(0,x) - \sin^2\alpha},$$
$$\Lambda_0^{\pm}(x) = C\partial_x(n^2(0,x)). \tag{42}$$

The constant is determined by the boundary conditions described in Section 4.1.

A similar stationary equation can be used for $Z^{\pm}$. However, assuming the incident energy only flows across the boundary $x = 0, z > 0$, we have $Z^-(0,0) = 0$ and the initial data can be identically set to 0.

4.3. Change of variable

We also, as in [3], use the following change of variables:

$$\tilde{x}(z,x) = x - x_c(z) + C_0, \tag{43}$$

where C_0 is the position of the caustic of the pseudo-stationary problem in $z < 0$, and thus the initial position $x_c(0) = C_0$ of the caustic. This change of variable simplifies the geometry of our computational domain, and makes its discretization easier. In the new variable $\tilde{x}$, the caustic is simply a straight line $\tilde{x} = C_0$. Setting $\tilde{U}^{\pm}(z,\tilde{x}) = U^{\pm}(z,x)$ and $\tilde{\phi}^{\pm}(z,\tilde{x}) = \phi^{\pm}(z,x)$ the generic transport equation (29) becomes

$$\partial_z\tilde{U}^{\pm} + (H_p(z,\tilde{x} + x_c(z) - C_0, \partial_{\tilde{x}}\tilde{\phi}^{\pm}) - \dot{x}_c(z))\partial_{\tilde{x}}\tilde{U}^{\pm} = f(\tilde{U}^{\pm}(z,\tilde{x})).$$

In particular, in the case of the geometrical spreading, Eq. (40) becomes, with simplified notations,

$$\partial_z\tilde{U} + V(z,\tilde{x})\partial_{\tilde{x}}\tilde{U} = A(z,\tilde{x})\tilde{U},$$

where

$$\tilde{U}^{\pm} = \begin{pmatrix} \tilde{\Theta}^{\pm} \\ \tilde{\Lambda}^{\pm} \end{pmatrix}, \quad V^{\pm}(z,\tilde{x}) = H_p(z,\tilde{x} + x_c(z) - C_0, \partial_{\tilde{x}}\tilde{\phi}^{\pm}) - \dot{x}_c(z),$$
$$A^{\pm}(z,\tilde{x}) = \begin{pmatrix} H_{xp}(z,\tilde{x} + x_c(z) - C_0, \partial_{\tilde{x}}\tilde{\phi}^{\pm}) & H_{pp}(z,\tilde{x} + x_c(z) - C_0, \partial_{\tilde{x}}\tilde{\phi}^{\pm}) \\ -H_{xx}(z,\tilde{x} + x_c(z) - C_0, \partial_{\tilde{x}}\tilde{\phi}^{\pm}) & -H_{xp}(z,\tilde{x} + x_c(z) - C_0, \partial_{\tilde{x}}\tilde{\phi}^{\pm}) \end{pmatrix}.$$

More precisely, $\tilde{\Theta}^{\pm}$ and $\tilde{\Lambda}^{\pm}$ are the solutions of

$$\begin{aligned} &\partial_z\tilde{U}^- + V^-(z,\tilde{x})\partial_{\tilde{x}}\tilde{U}^- = A^-(z,\tilde{x})\tilde{U}^-, \\ &\partial_z\tilde{U}^+ + V^+(z,\tilde{x})\partial_{\tilde{x}}\tilde{U}^+ = A^+(z,\tilde{x})\tilde{U}^+, \\ &\tilde{U}^+(z,x_c(z)) = \tilde{U}^-(z,x_c(z)), \\ &+\text{initial, incoming and outgoing conditions.} \end{aligned} \tag{44}$$

Remark. Since $\dot{x}_c(z) = H_p(z,x_c(z),p_c(z))$ where $p_c(z) = \partial_x\phi^{\pm}(z,x_c(z))$ (see (23)), the advection fields $V^{\pm}$ vanish at the caustic, which produces the numerical difficulties exposed below. This is not a side effect of the change of variables since it expresses following the geometrical property: at the

caustic, the advection fields $V^{\pm}$ are parallel to the caustic. A more precise result (proved in [3]) shows that the gradient of the phases $\phi^{\pm}$ behaves as a square root with respect to x in the vicinity of the caustic, i.e., at z fixed

$$\nabla\phi^{\pm}(z,x) = p_c(z) \pm B\sqrt{x_c(z) - x} + \mathrm{O}(x_c(z) - x)$$

with $B \neq 0$. Plugging this expression into V yields

$$V^{\pm}(z,\tilde{x}) = \pm BH_{pp}(z, x_c(z), p_c(z))\sqrt{C_0 - \tilde{x}} + \mathrm{O}(C_0 - \tilde{x}). \tag{45}$$

The strict convexity of H ensures that $H_{pp} > 0$. Therefore, the leading coefficient does not vanish and $V^{\pm}$ behaves as square root in the vicinity of the caustic. We examine the consequences of this singularity on the numerical schemes below.

5. Numerical scheme for the transport equations

Let $\{\tilde{x}_1, \ldots, \tilde{x}_J\}$ be a regular discretization of $[0, C_0]$. The z discretization $\{z^n\}$ follows by application of a CFL-type condition, depending on the angle of the rays with the x-axis (the smaller this angle, the stricter the CFL condition). Let δz and δx be the steps of discretization.

The value of a function a at point $(z^n, \tilde{x}_j)$ is denoted a_j^n, and $\partial_{\tilde{x}}^l a_j^n$ and $\partial_{\tilde{x}}^r a_j^n$ stand for its numerical discrete left and right derivatives. Upwind derivative operators of order 1 are

$$\partial_{\tilde{x}}^l a_j^n = \frac{a_j^n - a_{j-1}^n}{\delta x},$$

$$\partial_{\tilde{x}}^r a_j^n = \frac{a_{j+1}^n - a_j^n}{\delta x}.$$

5.1. Difficulties with the discretization

To illustrate the difficulties involved with the resolution of the transport equations in the vicinity of the caustic, we focus on the transport of the geometrical spreading (44). The numerical resolution of the Eikonal equations (23) is discussed in [3]. We therefore assume that the coefficients $V^{\pm}$ and $A^{\pm}$ are given. The problem of the Z transport equations (38) is similar.

Let us consider a usual first-order explicit discretization of the transport equations (44) as in [4], for instance,

$$\frac{U_j^{n+1} - U_j^n}{\delta z} + V_j^n \cdot \partial_x U|_j^n = A_j^n U_j^n, \tag{46}$$

where $\partial_x U|_j^n$ stands for the discrete derivative of U upwinded according to the sign of V_j^n. The classical convergence study (see [4] for example) does not apply here as our advection field has a singularity (it vanishes at the caustic as a square root as pointed by (45)).

We simplify further and restrict ourselves to a "stationary" index, independent of z. In this case, we showed in [3] that with appropriate pseudo-stationary boundary conditions, the solution U does not depend on z. Then scheme (46) simplifies to $V_j \cdot \partial_x U|_j = A_j U_j$. At the caustic point $\tilde{x}_J = C_0$, we get $A_J U_J = 0$ since $V_J = 0$. The matrix A_J being invertible (compute H's second derivatives and use $p_c = 0$), this implies $U_J = 0$. Obviously we do not recover the right solution since $U = (\Theta, \Lambda)$ is the

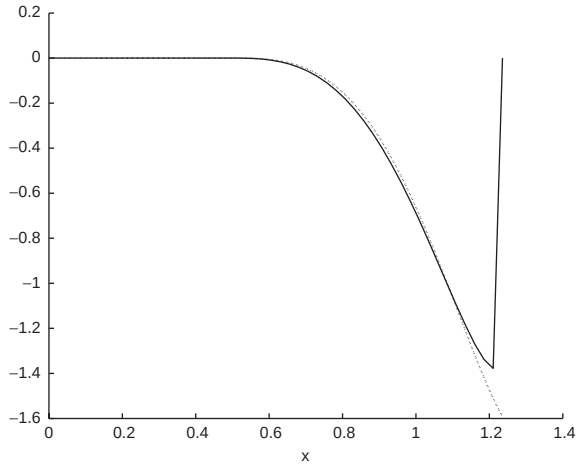

Fig. 9. Order 1 scheme.

Eulerian function corresponding to a nonzero solution of the linear system of ordinary differential equations (39), and therefore does not vanish.

In order to uphold numerically our discussion, we focus on index (48)

$$n(z,x) = \begin{cases} 1 & \text{if } x \leqslant 0.5, \\ 1-(x-0.5)^3. \end{cases}$$

As explained in [3], the phases $\phi^{\pm}$ can be computed exactly (up to a constant C ruled by (25)) through

$$\frac{\partial}{\partial x}\phi^{\pm} = \mp\sqrt{n^2(0,x) - \sin^2\alpha}.$$

Therefore, the computations discussed below have been carried out with the exact values of $V = H_p(0,x,\nabla\phi)$, thus proving that the difficulties encountered are not the consequence of errors that might have arisen in the former numerical resolution of the Eikonal equation.

Fig. 9 represents, in one dimension, the function Λ^- of x computed using scheme (46)—plain line—and the reference solution (42)—dotted line. As we approach the caustic, the two curves part, and the error is obvious at the caustic since Λ^- does not vanish there whereas scheme (46) produces $U_J = 0$. Increasing the order of the derivative operator to compute $\partial_x U|_j$ does not improve (as shown in Fig. 10) since $U_J = 0$ still at the caustic.

One can enhance things a little by shifting the computational grid of half a mesh so that the last mesh $x_J = C_0 - \frac{1}{2}\delta x$ is not on the caustic, and $V_J \neq 0$. Fig. 11 shows that the solution thus computed does no longer vanish at the caustic, but keeps on parting with the reference solution as one approaches the caustic. This suggests that the local behavior of V (as a square root) in the vicinity of the caustic, and not only its vanishing, accounts for the numerical difficulties. With second-order derivatives, we get the result of Fig. 12, somehow better, but still far from the accuracy required for the boundary condition on Λ^+ on the caustic derived from (30).

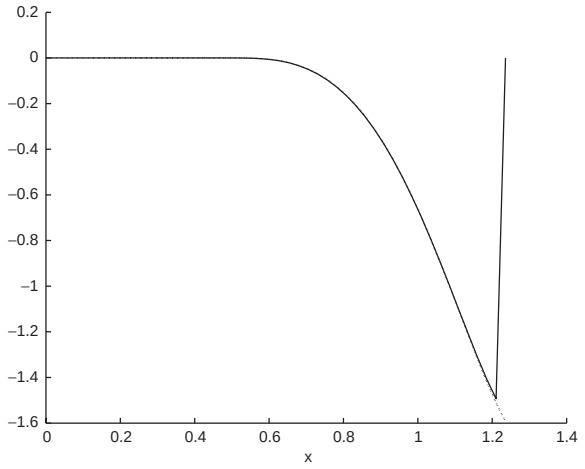

Fig. 10. Order 2 scheme.

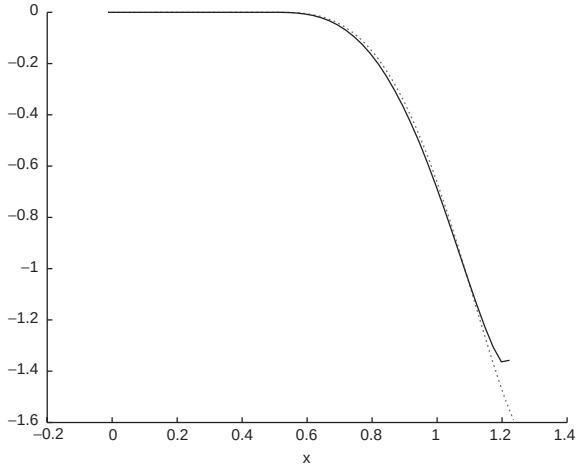

Fig. 11. Order 1 scheme with shifted grid.

5.2. Numerical scheme

Our proposed solution consists in averaging both the advection field V and the right-hand side AU according to the direction of the flow. The scheme we obtain is

$$\frac{U_j^{n+1}-U_j^n}{\delta z}+\frac{1}{2}(V_j^n+V_{j-1}^n)\frac{U_j^n-U_{j-1}^n}{\delta x}=\frac{1}{2}(A_j^nU_j^n+A_{j-1}^nU_{j-1}^n)$$

when $V_j^n>0$,

$$\frac{U_j^{n+1}-U_j^n}{\delta z}+\frac{1}{2}(V_j^n+V_{j+1}^n)\frac{U_{j+1}^n-U_j^n}{\delta x}=\frac{1}{2}(A_j^nU_j^n+A_{j+1}^nU_{j+1}^n)$$

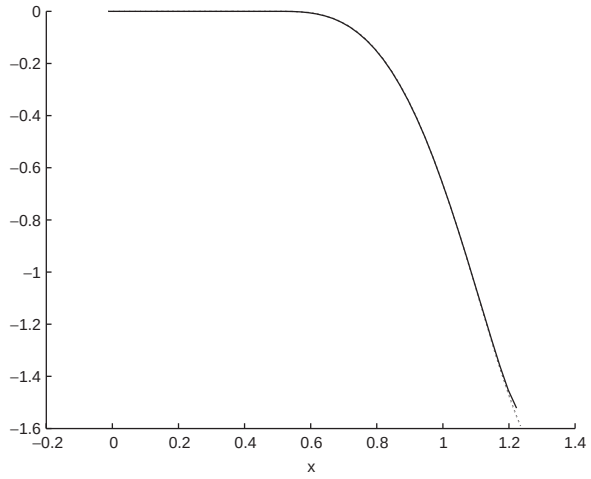

Fig. 12. Order 2 scheme with shifted grid.

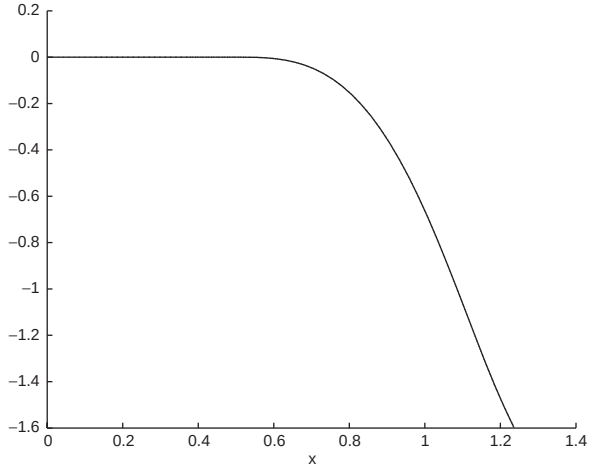

Fig. 13. Our scheme.

when $V_j^n < 0$ and simply

$$\frac{U_j^{n+1} - U_j^n}{\delta z} = A_j^n U_j^n$$

when $V_j^n = 0$.

We study this scheme in a simplified setting in Appendix A.2, and show that it is of order 2 away from the caustic, and degenerates only to order 1 in the vicinity of the caustic. We also show that schemes (46) degenerate from order 1 or 2 to 0.

Fig. 13 shows the reference and the computed solution, which are visually equal. The decisive test, described in Section 6.1, is to show that in genuinely two-dimensional cases, the

value of Λ^- we get on the caustic is accurate enough to allow the computation of Θ^+ and Λ^+ through (30).

6. Numerical results

In Sections 6.1 and 6.2, we compute numerically several functions such as $\Theta^\pm$ and $\Lambda^\pm$, and we check the convergence of our numerical methods as the discretization step tends to 0. We present a pointwise validation of formula (14) in Section 6.3. Then we check the theoretical asymptotic results (14) and (16) by letting k_0 to infinity (Section 6.4). We add some numerical computations in the case $v \neq 0$ in Section 6.5.

We first list several indexes that will be used for our numerical computations. The most simple is the stationary affine index that allows us to compute an analytically exact solution of the Helmholtz equation (1).

$$n^2(z,x) = 1 - x. \tag{47}$$

A slightly more realistic stationary index, modeling the propagation in a constant index media before entering the plasma where the ion density increases, is

$$n(z,x) = \begin{cases} 1 & \text{if } x \leqslant 0.5, \\ 1 - (x - 0.5)^3. \end{cases} \tag{48}$$

In this case, we use a finite difference scheme to compute a reference solution of (1) through its 1D simplification. We must however be careful that our verifications are not polluted by the numerical error of this method. We eventually add a z dependence as follows:

$$n(z,x) = \begin{cases} 1 & \text{if } x \leqslant 0.5, \\ 1 - (1 + 0.2z^2)(x - 0.5)^3 \end{cases} \tag{49}$$

and

$$n(z,x) = \begin{cases} 1 & \text{if } x \leqslant 0.5, \\ 1 - (1 + 0.3\sin z)(x - 0.5)^3. \end{cases} \tag{50}$$

In this case, it is not possible to compute reference solutions of the Helmholtz equation because of the computational cost at high frequencies.

6.1. Order of convergence

We examine the results of the scheme implemented to compute $\Theta^\pm$ and $\Lambda^\pm$ in a simple setting. We focus again on a pseudo-stationary case, with a (48)-type index, but in order to slightly complicate the situation, we tilt the axes at an angle β. More precisely, let us consider the change of coordinates:

$$x = X\cos\beta + Z\sin\beta,$$

$$z = -X\sin\beta + Z\cos\beta$$

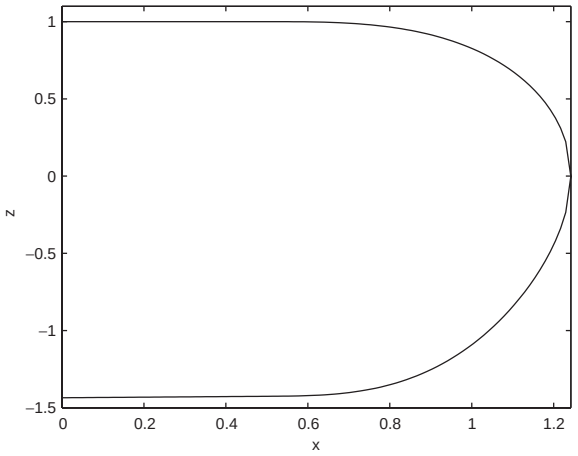

Fig. 14. Graphs of Θ^- and Θ^+, z fixed.

and an index of refraction that is stationary with respect to the (Z,X) variable, i.e., depending only on X:

$$n(Z,X) = \begin{cases} 1 & \text{if } X \leqslant 0.5, \\ 1-(X-0.5)^3. \end{cases}$$

We know from the study of stationary cases in [3] that an incoming plane wave induces an outgoing plane wave after touching the caustic, and this is not impaired by the change of variables. The geometric optics representation of a plane wave is characterized by a constant Θ and $\Lambda = 0$ (rays are parallel straight lines). This allows us to define the error made in the computation of $\Theta^{\pm}$ and $\Lambda^{\pm}$ as follows:

- the error on Θ will be the mean value of $|\Theta^-|$ on (a portion limited by z_0 and z_1 of) the caustic (recall that it is supposed to vanish there)

$$\int_{z_0}^{z_1} |\Theta^-(z, x_c(z))| \, \mathrm{d}z. \tag{51}$$

- the error on Λ will be the mean value of $|\Lambda^+|$ when leaving the domain at $x = 0$

$$\int_{z_0}^{z_1} |\Lambda^+(z,0)| \, \mathrm{d}z \tag{52}$$

(since a plane wave is supposed to flow out, this should also vanish).

The numerical results (Figs. 14 and 15) are computed with $J = 50$ points on the x-axis, an incoming angle $\alpha = \pi/4$, and $\beta = -\pi/24$. We impose $\Theta^- = 1$ and $\Lambda^- = 0$ (plane wave) on the incoming border Γ_{inc}. (The initial conditions are uniformly set to 0, but initial conditions are not a matter of importance with transport equations.) Since we are in a pseudo-stationary case, we only represent our results in one dimension, at constant z. Fig. 14 represents the graphs of $\Theta^{\pm}$. Fig. 15 shows the graphs of $\Lambda^{\pm}$. Note the continuity at the caustic.

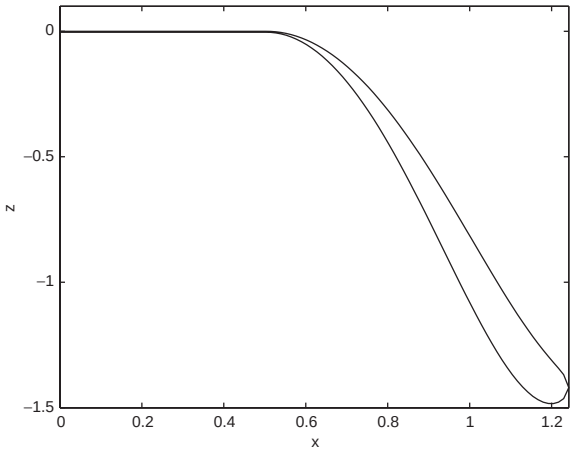

Fig. 15. Graphs of Λ^- and Λ^+, z fixed.

The array below shows the behavior of errors (51) and (52) versus the number of points J used to discretize the x-axis. Convergence is of order 1.

Behavior of the errors			
J	50	100	200
On Θ	0.0088	0.0043	0.0021
On Λ	0.0074	0.0038	0.0020

6.2. The energy computations

We now show how our method allows to compute the geometric optics approximation of the energy deposited by the laser in a certain domain. According to (16) this approximation is given as

$$\mathbb{E} = \int_D (|a^+|^2 + |a^-|^2) = \int_D \frac{Z^-}{\partial_z \phi^- |\Theta^-|} + \int_D \frac{Z^+}{\partial_z \phi^+ |\Theta^+|}. \tag{53}$$

In our computations below we take for D the whole computational domain (the illuminated region).

6.2.1. Numerical validation of (53)

We first consider the toy problem with index (47) for which we know the theoretical value $\mathbb{E}_0$ of the integral (see Appendix A.3). The array below gives the difference between the computed and the theoretical value of the energy for different values of J.

J	25	50	100
$\mathbb{E}(J) - \mathbb{E}_0$	0.0113	0.0080	0.0056

As explained in Appendix A.3, the convergence is of order $\frac{1}{2}$.

For a general index, it is necessary to solve numerically the transport equations on $Z^{\pm}$.

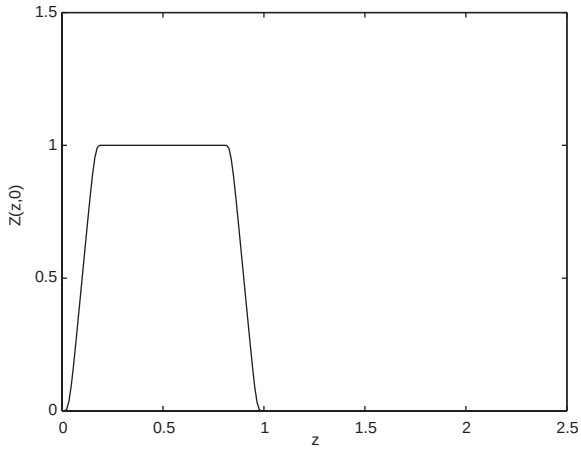

Fig. 16. Incoming Z on the z-axis.

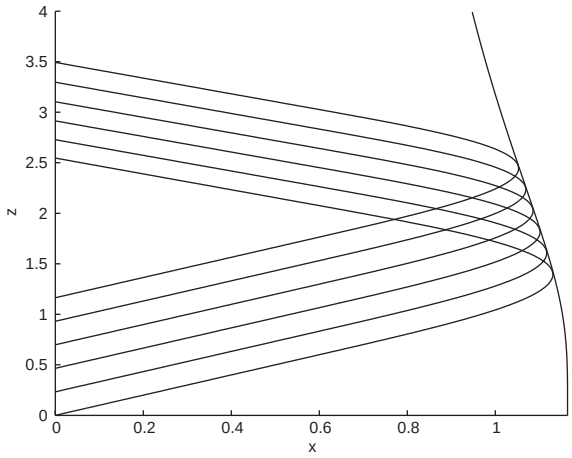

Fig. 17. Comparison with the ray method.

6.2.2. *The transport of Z*

We consider the index of refraction (49) and take an incoming angle $\alpha = \pi/4$. We solve Eq. (38) with $v = 0$ applying the numerical scheme described in Section 5. The incoming condition shown in Figs. 16 and 17 models a laser beam entering the plasma.

Fig. 18 represents the contour lines of Z^- and Z^+ superimposed. As Z is theoretically constant along the rays since $v = 0$, exact contour lines of Z are rays. The numerical solution is, however, polluted by the scheme's numerical diffusion. We can observed this phenomena by comparing the contour lines with the rays in Fig. (17). Fig. 19 illustrates a less dissipative Van Leer second order scheme.

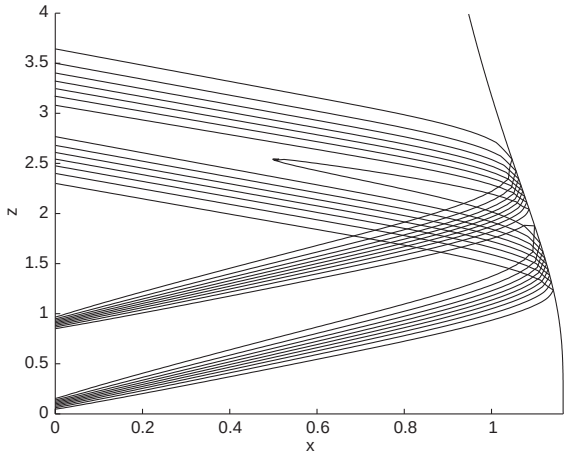

Fig. 18. Contour lines of Z^- and Z^+.

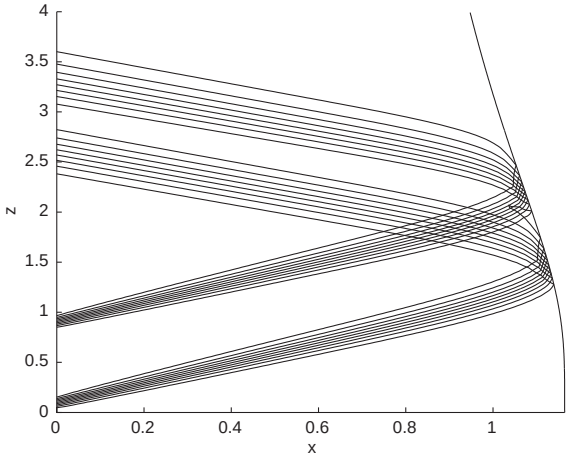

Fig. 19. Contour lines of Z^- and Z^+—Van Leer scheme.

The numerical pollution effect can be better observed by plotting the incoming and the outgoing beam on the x-axis. Since Z is constant along the rays ($v = 0$), the incoming plateau of Fig. 16 should be preserved between the two extremal rays but for the numerical diffusion. We first take $J = 50$ points discretization in x. In Fig. 20, we plot the incoming beam, i.e., $Z^-(0,z)$, with dots, and the outgoing beam, i.e., $Z^+(0,z)$, in plain line. In Fig. 21, the same but using a Van Leer-type second-order scheme. The plateau is better preserved since the peak reaches 0.85 in the second-order case instead of 0.77 in the first-order one. Finally, Fig. 22 shows the output of our scheme with $J = 300$ points discretization. Obviously, although converging, our scheme is not adapted for plateau transport (see [5] on this subject). Note (Section 6.1) that our scheme is first order for the transport of the geometrical spreading Θ.

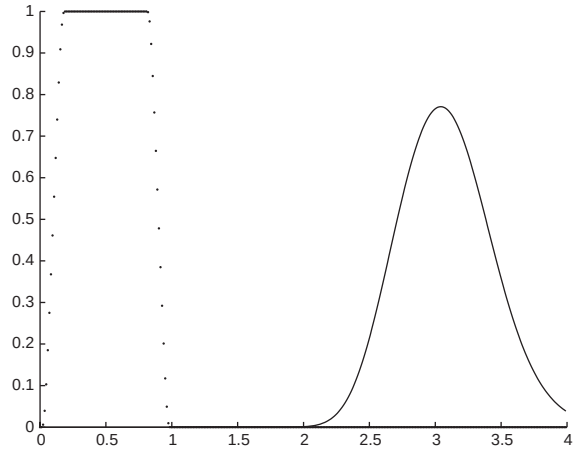

Fig. 20. Z^- and Z^+ on $x = 0$.

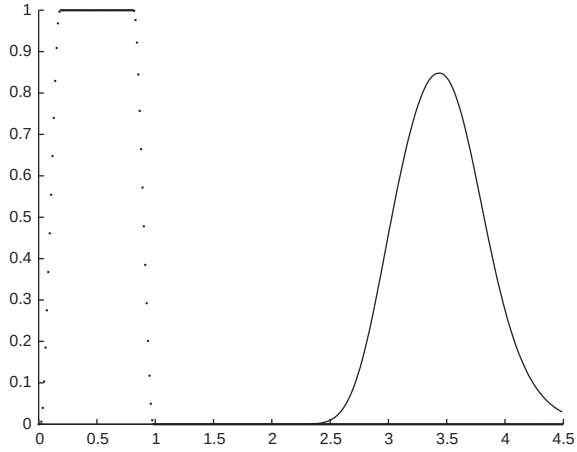

Fig. 21. Z^- and Z^+ on $x = 0$—Van Leer scheme, 50 points.

The energy computed with this numerical value of $Z^{\pm}$ converges, although we do not know its exact limit. The array below gives the energy deposited in the whole domain for different values of J. We observe in the table below that the error between two consecutive numerical solutions is first order. We can deduce that we have reached the limit by a 1% margin.

J	25	50	100	200
Energy $\mathbb{E}$	3.1167	3.1000	3.0941	3.0913

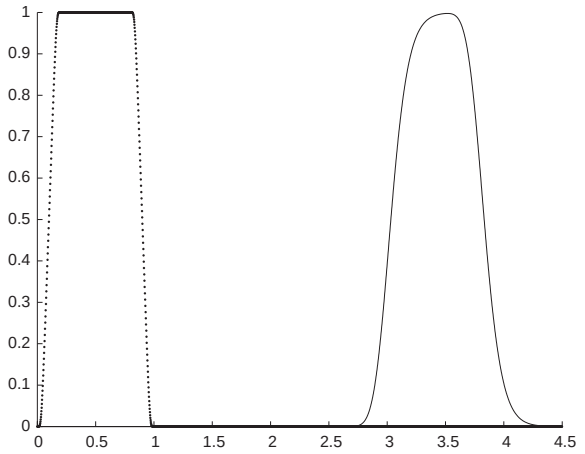

Fig. 22. Z^- and Z^+ on $x = 0$—Van Leer scheme, 300 points.

6.3. Numerical study of formula (14)

We now present numerical results which use the numerical output of our Eulerian numerical method to approximate the solution A of (1) by (14), still with no absorption. The amplitudes $a^{\pm}$ satisfy the real coefficient equations (6) with a possibly complex boundary data. In practice, however, we always choose a real positive incoming condition A_0 for the amplitudes $a^{\pm}$. They then remain real and are given by

$$a^{\pm} = \sqrt{E^{\pm}}. \tag{54}$$

The first comparison is in our affine index case (47) for which we have an analytical solution. Figs. 23–25 plot the real and the imaginary part of both the exact (plain line) and the numerical (stars) solution (as functions of x, z being fixed) for different frequencies. One sees the typical blow up of the GO ansatz at the caustic. Note that only one geometrical optics computation is necessary to compute approximation (14) for any frequency (indeed the discretization of the GO ansatz—the stars—does not change).

The second comparison uses the slightly more realistic index (48). This time the "exact" solution of the Helmholtz equation is computed using a given finite difference scheme which is responsible for additional errors. In this case, we were only able to compare the modulus of the solution for the following reason:

Recall that in the 1D case and for $v = 0$, $a^+ = a^-$ (see [3]; see also (13)). Then

$$\begin{aligned} A &= a^- \mathrm{e}^{-\mathrm{i}\pi/4} \exp(\mathrm{i}k_0\phi^-) + a^+ \mathrm{e}^{\mathrm{i}\pi/4} \exp(\mathrm{i}k_0\phi^+) = a^- \mathrm{e}^{-\mathrm{i}\pi/4}(\exp(\mathrm{i}k_0\phi^-) + \mathrm{i}\exp(\mathrm{i}k_0\phi^+)) \\ &= a^- \mathrm{e}^{-\mathrm{i}\pi/4} \exp \mathrm{i}\left(k_0 \frac{\phi^+ + \phi^-}{2} + \frac{\pi}{4}\right) \left[\exp \mathrm{i}\left(k_0 \frac{\phi^- - \phi^+}{2} - \frac{\pi}{4}\right) + \exp \mathrm{i}\left(k_0 \frac{\phi^+ - \phi^-}{2} + \frac{\pi}{4}\right)\right] \\ &= 2a^- \mathrm{e}^{-\mathrm{i}\pi/4} \exp \mathrm{i}\left(k_0 \frac{\phi^+ + \phi^-}{2} + \frac{\pi}{4}\right) \cos\left(k_0 \frac{\phi^+ - \phi^-}{2} + \frac{\pi}{4}\right). \end{aligned}$$

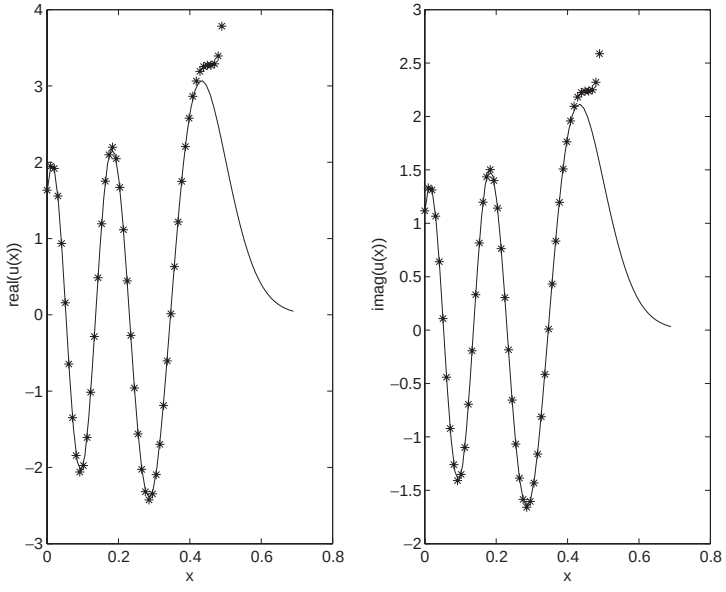

Fig. 23. Pointwise comparison in the (47) case–$k_0 = 60$.

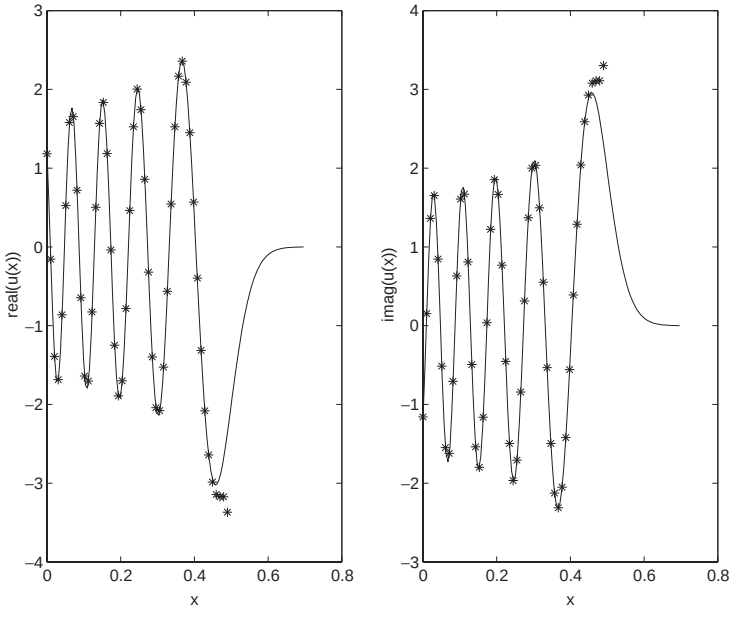

Fig. 24. Pointwise comparison in the (47) case–$k_0 = 120$.

Let us fix z. Also remember that in the 1D case, $(\phi^+ + \phi^-)/2 = z \sin\alpha + C$ (see [3]; see also (15)). We want to illustrate that a numerical error made on the computation of the phases may cause great distortion in a pointwise comparison. Let $\tilde{\phi}^{\pm}$ be the numerical outputs of our method. Let us now

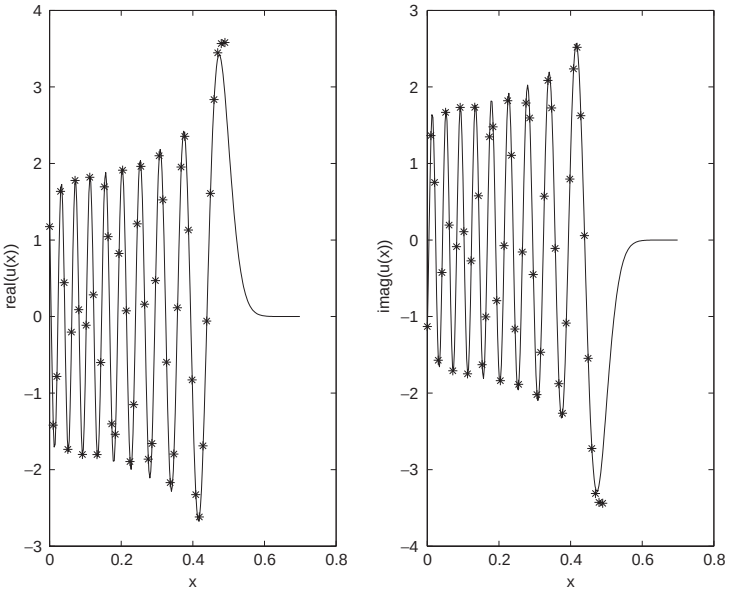

Fig. 25. Pointwise comparison in the (47) case–$k_0 = 240$.

choose k_0 such that $k_0(\tilde{\phi}^+(0) + \tilde{\phi}^-(0))/2 + \pi/4 \equiv \pi/2(2\pi)$. It cancels the real part of the numerical approximate GO ansatz at $x = 0$, and more or less everywhere. Because of the numerical errors on the phase the exact solution does not exactly satisfy, for the same k_0 : $k_0(\phi^+(0) + \phi^-(0))/2 + \pi/4 \equiv \pi/2(2\pi)$. So the real part of the exact solution does not vanish as we can see in Fig. 26 ($k_0 = 160$). We therefore only plot the moduli of the GO ansatz and the exact solution of the Helmholtz equation. Indeed,

$$|A|^2 = 2|a^-|^2 \cos^2\left(k_0 \frac{\phi^+ - \phi^-}{2} + \frac{\pi}{4}\right).$$

Now in a pointwise comparison of the moduli, we only get an phase error. Fig. 27 plots the modulus of the "exact" solution—plain line—versus the modulus of GO ansatz—stars—for $k_0 = 160$ (compare with Fig. 26). Figs. 28–30 correspond different values of k_0.

We finally consider index (50) for which the caustic is not a straight line. We only show the GO solution as direct resolutions of (1) are too expensive computationally. Fig. 32 shows the contour lines of the ansatz (14) evaluated through a computation of the GO problem using 50 points in x. One can observe the compression or dilation effects produced by the heterogeneous plasma.

6.4. Asymptotic convergence

We would like to check numerically the asymptotic convergence predicted by formulae (14) and (16) when $k_0 \to +\infty$. We can compute reference solutions for index (47) and (48). One must be careful that the numerical errors in the approximation of the GO solution does not pollute the

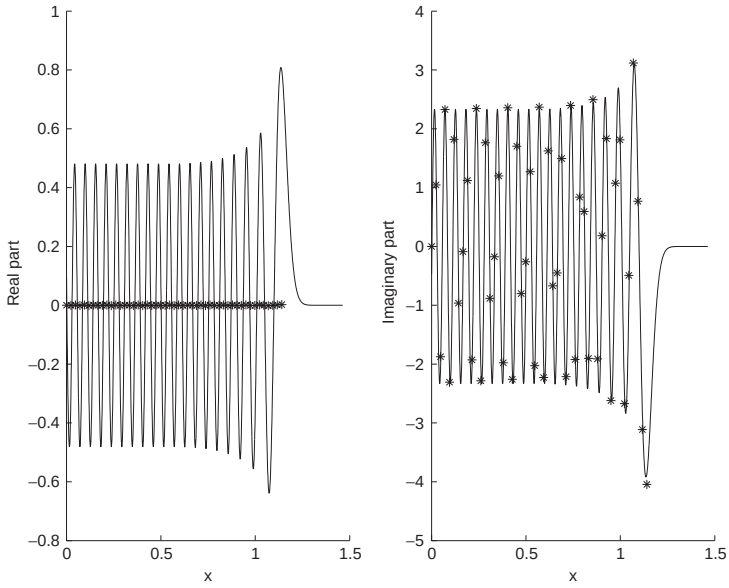

Fig. 26. Pointwise comparison in the (48) case–$k_0 = 160$.

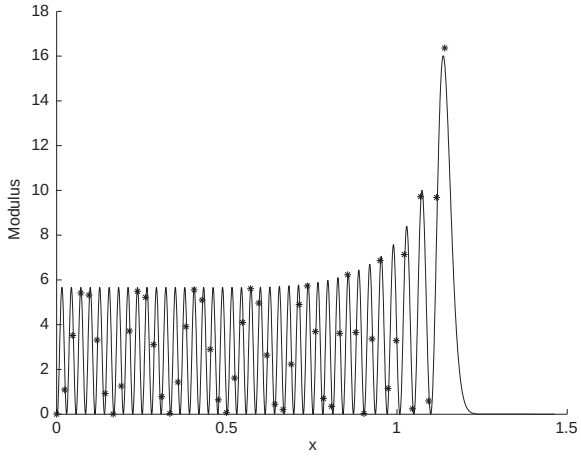

Fig. 27. Pointwise modulus comparison in the (48) case–$k_0 = 160$.

asymptotic error. In other words we must make sure that this error, depending on δx, is less than $O(k_0^{-1})$ for (14) and $O(k_0^{-1/3})$ for (16).

Formula (14): Let A be the exact solution to (1). Let A^{k_0} be its geometrical optics approximation in (14),

$$A^{k_0} = \frac{C}{2\sqrt{\pi}}\{a^- e^{-i\pi/4} \exp(ik_0\phi^-) + a^+ e^{i\pi/4} \exp(ik_0\phi^+)\}.$$

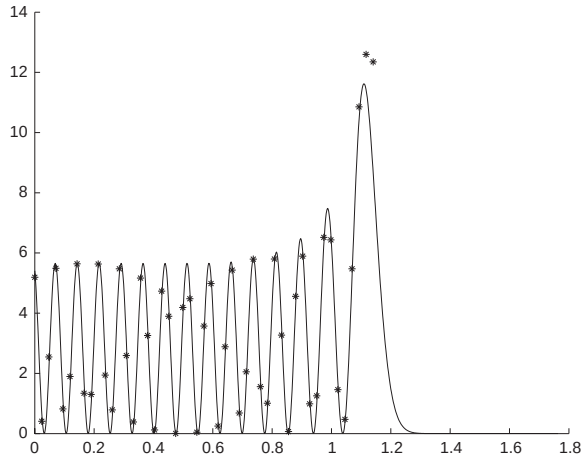

Fig. 28. Pointwise modulus comparison in the (48) case–$k_0 = 60$.

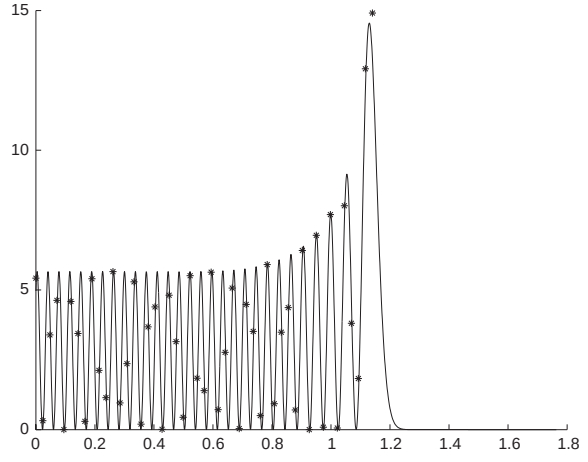

Fig. 29. Pointwise modulus comparison in the (48) case–$k_0 = 120$.

Formula (14) claims that, away from the caustic,

$$\|A - A^{k_0}\| = \mathrm{O}(k_0^{-1}),$$

where $\|.\|$ is the L^∞ norm in a closed region included in $x - x_c < \theta_0 < 0$ (i.e., strictly away from the caustic).

Let $h = \delta x$ be our discretization step. We denote by $\phi_h^\pm$ and $a_h^\pm$ the outputs of our numerical scheme. We showed in [3] (for ϕ) and in this paper (for a) that the numerical approximations are of order 1:

$$\|\phi^\pm - \phi_h^\pm\| = \mathrm{O}(h),$$

$$\|a^\pm - a_h^\pm\| = \mathrm{O}(h).$$

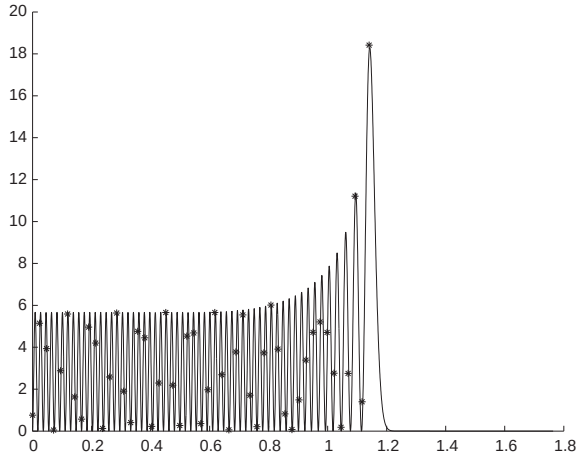

Fig. 30. Pointwise modulus comparison in the (48) case–$k_0 = 240$.

We finally denote by $A_h^{k_0}$ the numerical geometric optics approximation of A,

$$A_h^{k_0} = \frac{C}{2\sqrt{\pi}}\{a_h^- \mathrm{e}^{-\mathrm{i}\pi/4} \exp(\mathrm{i}k_0\phi_h^-) + a_h^+ \mathrm{e}^{\mathrm{i}\pi/4} \exp(\mathrm{i}k_0\phi_h^+)\}.$$

The numerical error made in the approximation of $a\exp(\mathrm{i}k_0\phi)$ by $a_h \exp(\mathrm{i}k_0\phi_h)$ can be estimated:

$$\begin{aligned}
&|a\exp(\mathrm{i}k_0\phi) - a_h\exp(\mathrm{i}k_0\phi_h)| \\
&\quad \leqslant |(a-a_h)\exp(\mathrm{i}k_0\phi)| + |a_h(\exp(\mathrm{i}k_0\phi) - \exp(\mathrm{i}k_0\phi_h))| \\
&\quad \leqslant \mathrm{O}(h) + |a_h\exp(\mathrm{i}k_0\phi)| \cdot |1 - \exp(\mathrm{i}k_0(\phi_h - \phi))| \\
&\quad \leqslant \mathrm{O}(h) + \mathrm{O}(1 - \exp(\mathrm{i}k_0\mathrm{O}(h))) \\
&\quad \leqslant \mathrm{O}(h) + \mathrm{O}(hk_0)
\end{aligned}$$

assuming that $hk_0 \to 0$. Taking the sum on $\pm$, we get

$$\|A^{k_0} - A_h^{k_0}\| \leqslant \mathrm{O}(h) + \mathrm{O}(hk_0).$$

We are interested in the convergence of $A_h^{k_0}$ towards A, so we consider

$$\begin{aligned}
\|A - A_h^{k_0}\| &\leqslant \|A - A^{k_0}\| + \|A^{k_0} - A_h^{k_0}\| \\
&\leqslant \mathrm{O}(k_0^{-1}) + \mathrm{O}(h) + \mathrm{O}(hk_0).
\end{aligned}$$

Theoretically, taking $h = \mathrm{O}(k_0^{-2})$ would allow to observe a convergence of $A_h^{k_0}$ towards A of order

$$\|A - A_h^{k_0}\| \leqslant \mathrm{O}(k_0^{-1}).$$

In practice, our Matlab cannot afford an $h = \mathrm{O}(k_0^{-2})$ discretization for large values of k_0. Given reasonable values of $h \sim 10^{-2}$, for large k_0 the $\mathrm{O}(hk_0)$ error is too important, and for smaller k_0 the $\mathrm{O}(k_0^{-1})$ error becomes important.

We nevertheless give numerical results in the array below, computed with the (47) index, showing the errors as a function of k_0. The error is the maximum pointwise error away from the caustic where we know (14) to be inaccurate. We chose to privilege large values of k_0, thus causing a large $O(hk_0)$ error. Note this time that we must rerun the GO computation for each k_0 evaluation.

k_0	J	$\|A - A_h^{k_0}\|$	$\|A - A^{k_0}\|$	$\|A^{k_0} - A_h^{k_0}\|$
200	50	0.1412	0.0422	0.1465
400	200	0.0363	0.0287	0.0360

The error made in the numerical approximation of A^{k_0} by $A_h^{k_0}$, due to the $O(hk_0)$ term, is much larger than the geometric optics approximation theoretical $O(k_0^{-1})$ error for $k_0 = 200$ and $J = 50$. On the next step, where $k_0 = 400$ and $J = 200$, both errors are comparable. Unfortunately, we were not able to compute the following step $k_0 = 800$ and $J = 800$, which should allow to observe the $O(k_0^{-1})$ error in $\|A - A_h^{k_0}\|$. We finally note that the range of k_0 is yet too small to observe a truly $O(k_0^{-1})$ convergence of $\|A - A^{k_0}\|$ (the error is not quite divided by 2).

In the second case (48), neither the theoretical values of the asymptotic approximation A^{k_0} nor the exact solution A can be computed. As the $h = O(k_0^{-2})$ discretization imposed to prevent numerical errors from polluting the asymptotic approximation is much stricter than $h = O(k_0^{-1})$ we can use the finite difference solution of the Helmholtz equation (1) as an approximation of A. So, we still can try to verify the estimate $\|A - A_h^{k_0}\| \leqslant O(k_0^{-1}) + O(h) + O(hk_0)$. The $O(h)$ error comes from the numerical error made in the computation of the amplitudes, whereas the $O(hk_0)$ error is due to the numerical error on the phases. In this case, the error we make in the computation of the phase is such that, for reasonable values of $h \sim 10^{-2}$, the $O(hk_0)$ error is too large to allow a pointwise comparison. Indeed, Figs. 31 and 32 compares the GO ansatz, computed with a $J = 200$ points discretization in x, and the "exact" solution of the Helmholtz equation for $k_0 = 60$. Even at this low frequency, results are not visually satisfactory (check the extremal points of the imaginary part). The array below gives the numerical results.

k_0	J	$\|A - A_h^{k_0}\|$
200	50	0.6179
400	200	0.3419

Formula (16): The discretization error in (53) being of order $O\left(\sqrt{\delta x}\right)$ (see Appendix A.3), we need $\sqrt{\delta x} = O(k_0^{-1/3})$ to verify (16). We take $\delta x = k_0^{-2/3}$. The array below shows the difference between the energy of the solution A of (1), that is the integral of $|A|^2$, and the output of our numerical scheme. Both converge towards the exact value of (53), but we check the rate of convergence, which is indeed found to be of order $O(k_0^{-1/3})$.

k_0	125	350	1000
Error	0.0114	0.0080	0.0056

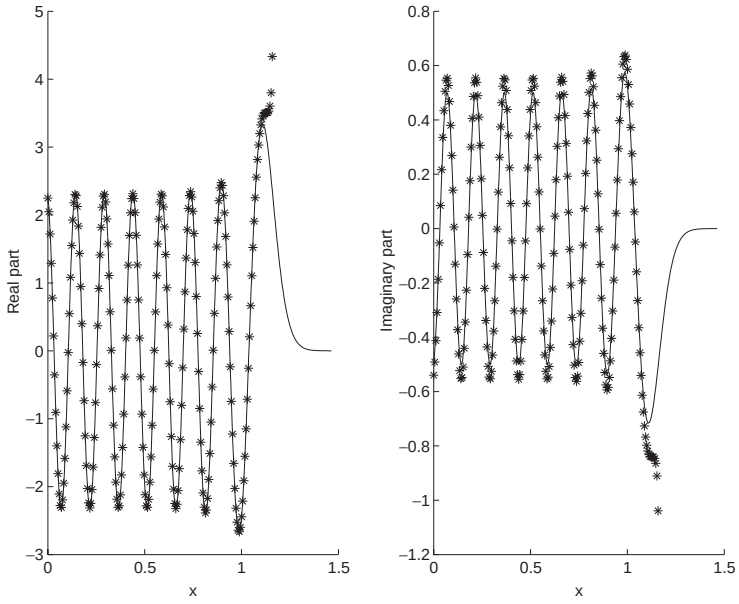

Fig. 31. Pointwise comparison in the (48) case–$k_0 = 60$.

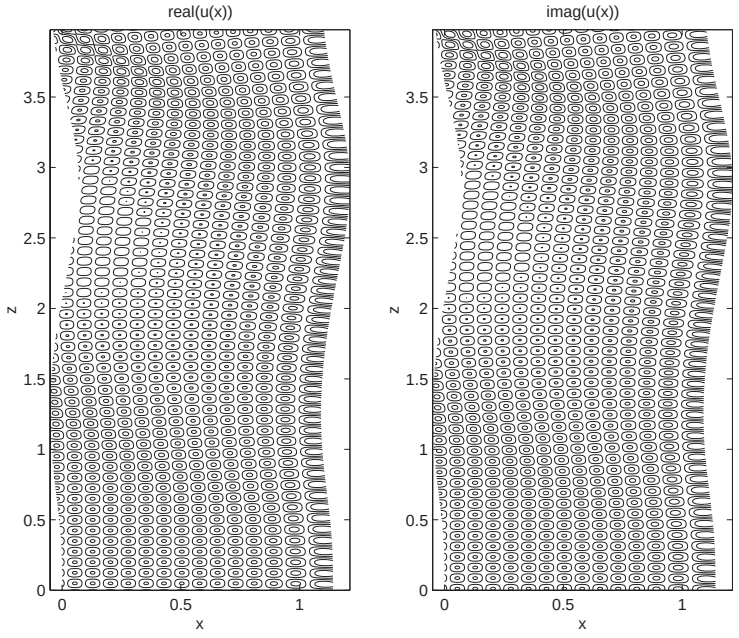

Fig. 32. The (14) ansatz.

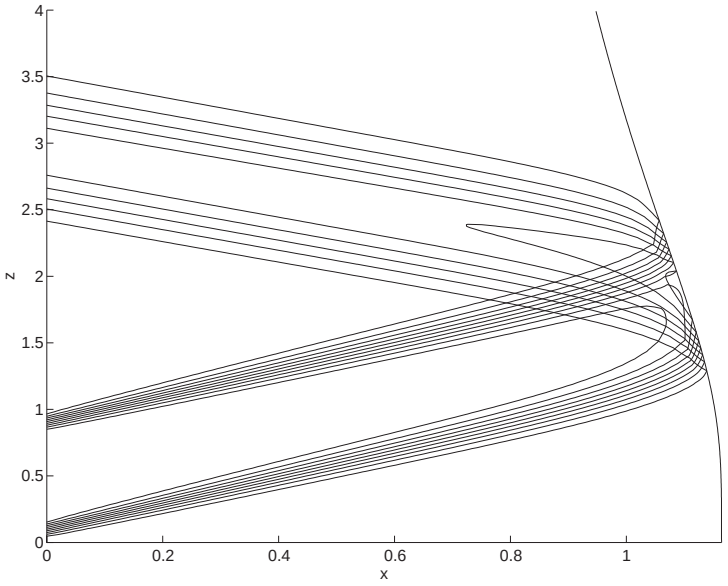

Fig. 33. The contour lines of $Z^{\pm}$ with absorption.

6.5. A $v \neq 0$ case

We finally give numerical results in a case where the absorption parameter is nonconstant. A physically relevant formula is $v = v_0(1 - n^2)$ with $v_0 = 0.7$. We consider the incoming beam of Fig. 16 propagating in the (49) index. Fig. 33 represents the contour lines of Z^- and Z^+ superimposed. Note how Z diminishes in the vicinity of the caustic (where the electronic density N and thus the absorption coefficient v are the highest). Indeed, four contour lines close up instead of one (due to numerical diffusion) in the no absorption case of Fig. 19. Fig. 34 represents the numerical realization of ansatz (14). One checks both the energy concentration in the vicinity of the caustic and the absorption effect of the plasma.

Appendix A

A.1. Details on the solution of (9)

The index of refraction is given by (8). The analytical solutions for the phase and amplitude are given in introduction (15), (13).

We denote the energy of the 1D solution u in an interval $[x_1, x_2]$ by $\mathscr{H}_{x_1,x_2}$, where

$$\mathscr{H}_{x_1,x_2} = \int_{x_1}^{x_2} |u(x)|^2 \, \mathrm{d}x.$$

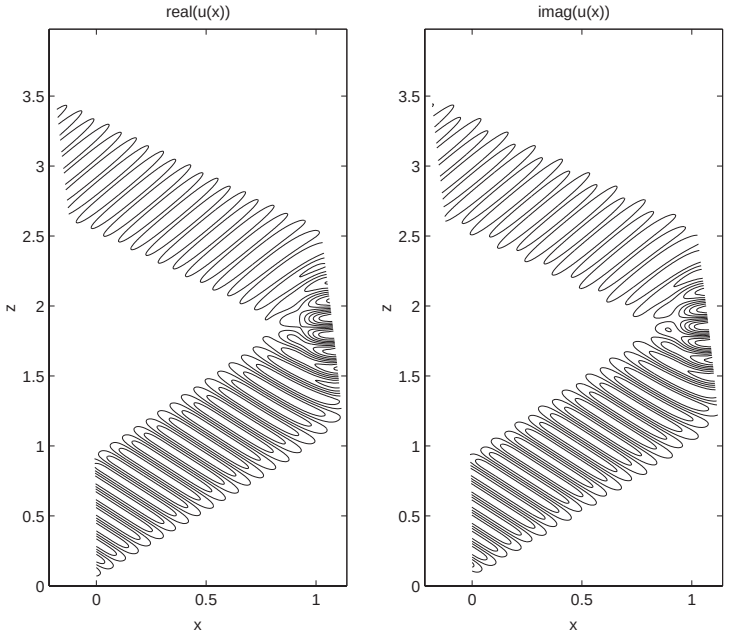

Fig. 34. The (14) ansatz with absorption.

In this case the solutions of (A.9) are explicit:

$$\Theta^- = |\Theta^+| = \sqrt{\frac{x_c - x}{x_c}}$$

and the equations on $Z^{\pm}$ (A.10) simplify

$$vZ^- + \sqrt{x_c - x}\frac{\partial Z^-}{\partial x} = 0, \quad Z^-(0) = \sin\alpha,$$

$$vZ^+ - \sqrt{x_c - x}\frac{\partial Z^+}{\partial x} = 0, \quad Z^+(x_c) = Z^-(x_c).$$

The solution is again explicitly given:

$$Z^-(x) = \exp\left(-2v\sqrt{x_c} + 2v\sqrt{x_c - x}\right)\ \sin\alpha,$$

$$Z^+(x) = \exp\left(-2v\sqrt{x_c} - 2v\sqrt{x_c - x}\right)\ \sin\alpha.$$

We now want to check the validity of the energy formula (37) in this case. As the index is independent of z, it is sufficient to examine the simplified energy relation

$$\mathscr{H}_{x_1,x_2} = \int_{x_1}^{x_2} |u(x)|^2\,\mathrm{d}x \simeq \int_{x_1}^{x_2} \left(\frac{Z^-}{\sin\alpha\Theta^-} + \frac{Z^+}{\sin\alpha|\Theta^+|}\right)\mathrm{d}x \tag{A.1}$$

in an interval $[x_1, x_2]$. We have the following:

Proposition. *For any x_1, x_2 in the interval $[0, x_c]$, (A.1) holds when k_0 goes to infinity. It proves in particular that the integral is convergent when $x_2 = x_c$.*

Let us first state the following technical result:

Lemma 1. *For ζ real positive number going to ∞ and ω positive real number bounded, we have*

$$|(\mathbf{Ai}(-(\zeta+\mathrm{i}\omega))|^2 = \zeta^{-1/2}\frac{1}{2\pi}\left(\cosh(2\zeta^{1/2}\omega) - \sin\left(\frac{4}{3}\zeta^{3/2}\right)\right)(1+\mathrm{o}(\zeta^{-1})).$$

Proof of the proposition. We will use the scaling

$$w(\zeta) = u(x), \quad \zeta = (x_c - x)k_0^{2/3},$$

where u is the solution of the 1D problem (9) specified in the introduction. We set the scaled parameters $\hat{v} = vk_0^{-1/3}$ and $\zeta_L = (\cos^2\alpha)k_0^{2/3}$ (corresponding to $x = 0$). Then if we neglect the B_i contribution as discussed in the introduction the solution can be written

$$u(x) = Ck_0^{1/6}\mathbf{Ai}(-k_0^{2/3}(x_c - x) + vk_0^{-1/3}) \tag{A.2}$$

or

$$w(\zeta) = Ck_0^{1/6}\mathbf{Ai}(-\zeta - \mathrm{i}\hat{v}). \tag{A.3}$$

The radiation boundary condition (10) can then be reduced to a transparent boundary condition in the constant index zones and we obtain at $\zeta = \zeta_L$ ($x = 0$):

$$\left[w + \frac{\mathrm{i}k_0^{-1/3}}{\cos\alpha}\frac{\partial w}{\partial\zeta}\right]_{\zeta_L} = 2. \tag{A.4}$$

The boundary condition (A.4) can now be used to evaluate the constant C. According to the classical asymptotic expansion of the Airy function (see e.g., [1]), we know that

$$w(\zeta) \simeq \frac{Ck_0^{1/6}}{\sqrt{\pi}(\zeta+\mathrm{i}\hat{v})^{1/4}}\sin\left(\frac{2}{3}(\zeta+\mathrm{i}\hat{v})^{3/2} + \frac{\pi}{4}\right),$$

$$(\partial_\zeta w)(\zeta) \simeq \frac{Ck_0^{1/6}}{\sqrt{\pi}(\zeta+\mathrm{i}\hat{v})^{1/4}}\cos\left(\frac{2}{3}(\zeta+\mathrm{i}\hat{v})^{3/2} + \frac{\pi}{4}\right)(\zeta+\mathrm{i}\hat{v})^{1/2}.$$

Since $(\zeta_L + \mathrm{i}\hat{v})^{1/4} = (\cos\alpha)^{1/2}k_0^{1/6}(1 + \mathrm{O}(k_0^{-1}))$, we get

$$\left[w + \frac{\mathrm{i}k_0^{-1/3}}{\cos\alpha}(\partial_\zeta w)\right]_{\zeta_L}$$

$$\simeq \frac{C}{\sqrt{\pi}\cos^{1/2}\alpha}\left(\sin\left[\frac{2}{3}(\zeta_L+\mathrm{i}\hat{v})^{3/2} + \frac{\pi}{4}\right] + \mathrm{i}\cos\left[\frac{2}{3}(\zeta_L+\mathrm{i}\hat{v})^{3/2} + \frac{\pi}{4}\right]\right).$$

Now according to condition (A.4) we must have

$$4 = \frac{|C|^2}{\pi\cos\alpha}\left|\exp\left(-\mathrm{i}\frac{2}{3}(\zeta_L+\mathrm{i}\hat{v})^{3/2}\right)\right|^2 = \frac{|C|^2}{\pi\cos\alpha}\exp\left(\frac{4}{3}\,\mathrm{Im}((\zeta_L+\mathrm{i}\hat{v})^{3/2})\right).$$

Since $\zeta_L^{1/2}\hat{v} = v\cos\alpha$, we see according to (A.7) that,

$$|C|^2 = 4\pi e^{-2v\cos\alpha}\cos\alpha. \tag{A.5}$$

Now, we focus on the evaluation of $\mathscr{H}_{x_1,x_2}$. According to Lemma 1, we see that for any x_1, x_2 smaller than x_c:

$$\begin{aligned}\mathscr{H}_{x_1,x_2} &= k_0^{1/3}\int_{x_1}^{x_2} C^2|\mathbf{Ai}(-(x_c-x)k_0^{2/3} - i\hat{v})|^2\,dx \\ &\simeq \frac{C^2}{2\pi}\int_{x_1}^{x_2}(x_c-x)^{-1/2}\left(\cosh[2((x_c-x)k_0^{2/3})^{1/2}k_0^{-1/3}v] - \sin\left[\frac{4}{3}k_0(x_c-x)^{3/2}\right]\right)dx\end{aligned}$$

thus

$$\mathscr{H}_{x_1,x_2} \simeq \frac{C^2}{2\pi}\int_{x_1}^{x_2}\sqrt{\frac{x_c}{x_c-x}}\cosh[2v(x_c-x)^{1/2}]\,dx.$$

That is to say (A.1). □

Proof of the lemma. We know, according to [1] for example, that

$$\mathbf{Ai}(-(\zeta+i\omega)) = \frac{(\zeta+i\omega)^{-1/4}}{\sqrt{\pi}}\sin\left(\frac{2}{3}(\zeta+i\omega)^{3/2}+\pi/4\right)(1+o((\zeta+i\omega)^{-1})). \tag{A.6}$$

Thus, we get

$$\begin{aligned}|\mathbf{Ai}(-(\zeta+i\omega))|^2 = \frac{(\zeta+i\omega)^{-1/2}}{2\pi}&\left(\cosh\left(\frac{4}{3}\,\mathrm{Im}((\zeta+i\omega)^{3/2})\right.\right. \\ &\left.\left.+\sin\left(\frac{4}{3}\,\mathrm{Re}((\zeta+i\omega)^{3/2})\right)\right)(1+o(\zeta^{-1}))\right).\end{aligned}$$

Since we have

$$\begin{aligned}&\mathrm{Im}((\zeta+i\omega)^{3/2}) = |\zeta^2+\omega^2|^{3/2}\sin\left(\frac{3}{2}\,\mathrm{arctg}\,\frac{\omega}{\zeta}\right) = \frac{3}{2}\,\zeta^{1/2}\omega(1+o(\zeta^{-1})), \\ &\mathrm{Re}((\zeta+i\omega)^{3/2}) = \zeta^{3/2}(1+o(\zeta^{-1})),\end{aligned} \tag{A.7}$$

we see that

$$\begin{aligned}&\cosh\left(\tfrac{4}{3}\,\mathrm{Im}((\zeta+i\omega)^{3/2}\right) + \sin\left(\tfrac{4}{3}\,\mathrm{Re}((\zeta+i\omega)^{3/2})\right) \\ &\quad\simeq \left(\cosh(2\zeta^{1/2}\omega) + \sin\left(\tfrac{4}{3}\,\zeta^{3/2}\right)\right)(1+o(\zeta^{-1}))\big).\end{aligned}$$

Thus the desired result. □

A.2. Order of the schemes proposed in Section 5.2

We focus on a simplified version of transport equation (38), assuming that the solution only depends on x:

$$v(x)f'(x) = a(x)f(x), \tag{A.8}$$

where $v(x) \geqslant 0$ and f is a scalar function. We study the different numerical schemes proposed for this equation in Section 5. For each scheme, we first determine its order in the case where v is smooth. We then study the behavior of the truncation error near the caustic when $v(x)$ behaves as a square root as in (45). In that case we denote

$$v(x) = \sqrt{x_c - x}\, w(x),$$

where w is a nonvanishing C^∞ function.

Scheme 1 (*upwind*):

$$v(x)\frac{f(x) - f(x-h)}{h} = a(x)f(x).$$

Order of this scheme:

$$v(x)\frac{f(x) - f(x-h)}{h} - a(x)f(x) = -\frac{1}{2}f(x)R_1(x)h + \mathrm{O}(h^2),$$

where

$$R_1(x) = \frac{a'(x)v(x) - a(x)v'(x) + a(x)^2}{v(x)}.$$

When $v(x)$ behaves as a square root,

$$R_1(x) = \frac{2(x - x_c)(a(x)w'(x) + a'(x)w(x)) + 2\sqrt{x_c - x}a(x)^2 + a(x)w(x)}{2w(x)(x_c - x)}$$

and as $h \to 0$,

$$R_1(x_c - h)h \to \frac{a(x_c)}{2}.$$

Using an heuristic argument (see [3]), we claim that if a does not vanish at the caustic, this scheme does not converge as one approaches the caustic, since the remainder is of order O(1).

We study next a second-order scheme, but as we shall see, it still does not converge at the caustic.

Scheme 2 (*centered*):

$$v\left(x - \frac{1}{2}h\right)\frac{f(x) - f(x-h)}{h} = a\left(x - \frac{1}{2}h\right)\frac{f(x) + f(x-h)}{2}.$$

Order of this scheme:

$$v\left(x - \frac{1}{2}h\right)\frac{f(x) - f(x-h)}{h} - a\left(x - \frac{1}{2}h\right)\frac{f(x) + f(x-h)}{2}$$

$$= -\frac{1}{24}f(x)R_2(x)h^2 + \mathrm{O}(h^3),$$

where

$$R_2(x) = (6a'(x)a(x)v(x) + 2a(x)^3 + 2a''(x)v(x)^2 + 2a'(x)v'(x)v(x) + a(x)v''(x)v(x) - 2a(x)v'(x)^2)/v(x)^2.$$

In the case, where $v(x)$ behaves as a square root, the leading terms in R_2 are $v''v$ and v'^2: as $x \to x_c$,

$$R_2(x) \simeq a(x)\frac{v''(x)v(x) - 2v'(x)^2}{v(x)^2}$$

and as $h \to 0$,

$$R_2(x_c - h)h^2 \to -\frac{3}{4}a(x_c).$$

Again, if a does not vanish at the caustic, this scheme does not converge as one approaches the caustic.

We now study the scheme proposed in this article (Section 5.2), and show that the remainder remains of order 1 as we approach the caustic.

Scheme 3 (*our scheme*):

$$\frac{v(x) + v(x-h)}{2}\frac{f(x) - f(x-h)}{h} = \frac{a(x)f(x) + a(x-h)f(x-h)}{2}.$$

Order of this scheme:

$$\frac{v(x) + v(x-h)}{2}\frac{f(x) - f(x-h)}{h} - \frac{a(x)f(x) + a(x-h)f(x-h)}{2} = -\frac{1}{12}f(x)R_3(x)h^2 + \mathrm{O}(h^3),$$

where

$$R_3(x) = (3a'(x)a(x)v(x) + a(x)^3 + a''(x)v(x)^2 + a'(x)v'(x)v(x) - a(x)v''(x)v(x) - a(x)v'(x)^2)/v(x)^2.$$

For this scheme, in the case where $v(x)$ behaves as a square root, the key ingredient is that the leading terms $v''v$ and v'^2 simplify: $v''(x)v(x) + v'(x)^2 = 0$. Then

$$R_2(x) \simeq \frac{a(x)^3 + a'(x)v'(x)v(x)}{v(x)^2}$$

and as $h \to 0$,

$$R_2(x_c - h)h^2 = \mathrm{O}(h).$$

The scheme remains first order at the caustic.

A.3. Numerical integration

We want to compute

$$\mathbb{E} = \int_D \frac{Z^-}{\partial_z\phi^-|\Theta^-|} + \int_D \frac{Z^+}{\partial_z\phi^+|\Theta^+|}$$

in the (47) index case.

Solving (40) we get

$$\Theta^{\pm}(x) = \pm\frac{\cos\alpha}{\sqrt{\cos^2\alpha - x}}.$$

When the boundary condition on Z^- is uniformly constant and $v = 0$, $Z^{\pm}$ are constant. We also have $partial_z\phi^{\pm} = \sin\alpha$. So, up to a constant,

$$\mathbb{E} = \int_0^{\cos^2\alpha} \frac{1}{\sqrt{\cos^2\alpha - x}}\,\mathrm{d}x.$$

This formula allows to compute the exact value used for the numerical comparison in Section 6.2.

Moreover, we want to study how the integral $\mathbb{E}$ behaves through discrete integration of the exact function sampled at a δx step. Of course the main difficulty is that $\Theta^{\pm}$ vanishes at the caustic.

We focus on the simplified formula

$$\mathbb{E} = \int_0^1 \frac{1}{\sqrt{x}}\,\mathrm{d}x.$$

Let us study the convergence of the discrete integral

$$\mathbb{E}_n = \frac{1}{n}\sum_{k=1}^{n}\frac{1}{\sqrt{k/n}}.$$

Since $x \mapsto 1/\sqrt{x}$ decreases, we get

$$\int_{\frac{1}{n}}^{1+1/n} \leqslant \mathbb{E}_n \leqslant \int_0^1 \frac{1}{\sqrt{x}}\,\mathrm{d}x$$

and therefore

$$|\mathbb{E} - E_n| = \mathrm{O}\left(\sqrt{\frac{1}{n}}\right).$$

In the general case, in order to improve the precision, we use a specific evaluation in the last mesh and a trapezoidal interpolation elsewhere, but as illustrated by the numerical results in Section 6.2, we did not succeed in removing the $\mathrm{O}\left(\sqrt{\delta x}\right)$ behavior.

A.4. Direct derivation of (38)

We now define directly $Z^{\pm}$ by $Z^{\pm} = E^{\pm}|\Theta^{\pm}|\partial_z\phi^{\pm}$. We also set $T^{\pm} = |\Theta^{\pm}|\partial_z\phi^{\pm}$, then we get

Lemma 1. *When* (z,x) *in not close to* $\mathscr{C}$, *we have*

$$\nabla\phi^{\pm}\cdot\nabla T^{\pm} = T^{\pm}\nabla\cdot(\nabla\phi^{\pm}).$$

Proof. According to the definition of $\Theta^{\pm}$, we have the classical result

$$\partial_z\Theta^{\pm} = \Theta^{\pm}\partial_x\mathscr{V}^{\pm}.$$

In our case ($d = 1$), it is a simple consequence of the relation

$$\partial_z(\partial_{x_0}(y^{\pm}(z,x_0))) = \partial_{x_0}(\mathscr{V}^{\pm}(y^{\pm}(z,x_0))) = \partial_{x_0}(y^{\pm}(z,x_0))\frac{\partial \mathscr{V}^{\pm}}{\partial y}.$$

Then, according to relation (29), the Eulerian quantity $\Theta^{\pm}$ satisfies

$$\partial_z\Theta^{\pm} + \frac{\partial_x\phi^{\pm}}{\partial_z\phi^{\pm}}\,\partial_x\Theta^{\pm} = \Theta^{\pm}\partial_z\phi^{\pm}\partial_x\left(\frac{\partial_x\phi^{\pm}}{\partial_z\phi^{\pm}}\right)$$

that is to say

$$\nabla\phi^{\pm}\cdot\nabla\Theta^{\pm} = \Theta^{\pm}\partial_z\phi^{\pm}\partial_x\left(\frac{\partial_x\phi^{\pm}}{\partial_{x,z}\phi^{\pm}}\right). \tag{A.9}$$

Thus by multiplying by $\partial_z\phi^{\pm}$, we get

$$\partial_z\phi^{\pm}[\nabla\phi^{\pm}\cdot\nabla\Theta^{\pm}] = \Theta^{\pm}\partial_z\phi^{\pm}\nabla\cdot(\nabla\phi^{\pm}) - \Theta^{\pm}\partial_x\phi^{\pm}\partial_{x,z}\phi^{\pm} - \Theta^{\pm}\partial_z\phi^{\pm}\partial_{z,z}\phi^{\pm}.$$

Since $\partial_x\phi^{\pm}\partial_{x,z}\phi^{\pm} + \partial_z\phi^{\pm}\partial_{z,z}\phi^{\pm} = \nabla\phi^{\pm}\cdot\nabla(\partial_z\phi^{\pm})$.

We get the sought for equation

$$\nabla\phi^{\pm}\cdot\nabla(\Theta^{\pm}\partial_z\phi^{\pm}) = \Theta^{\pm}\partial_z\phi^{\pm}\nabla\cdot\nabla\Theta^{\pm}. \qquad \square$$

Proposition 1. *When (z,x) is not close to $\mathscr{C}$, we have*

$$vZ^{\pm} + \nabla\phi^{\pm}\cdot\nabla Z^{\pm} = 0 \tag{A.10}$$

This equation is equivalent to (38).

Proof. Multiplying relation (7) by $T^{\pm}$ yields

$$vZ^{\pm} + T^{\pm}\nabla\cdot(E^{\pm}\nabla\phi^{\pm}) = 0.$$

Thus, we get

$$vZ^{\pm} + E^{\pm}T^{\pm}\nabla\cdot(\nabla\phi^{\pm}) + T^{\pm}\nabla E^{\pm}\cdot\nabla\phi^{\pm} = 0$$

and using the previous lemma we get the result. $\square$

References

[1] M. Abramowitz, I.A. Stegun, Handbook of Mathematical Functions with Formulas, Graphs, and Mathematical Tables, Dover, New York, 1992 (MR 94b:00012).

[2] J.-D. Benamou, Direct solution of multi-valued phase-space solutions for Hamilton–Jacobi equations, Comm. Pure Appl. Math. 52 (1999) 1443–1475.

[3] J.-D. Benamou, O. Lafitte, R. Sentis, I. Solliec, A geometric optics method for high frequency electromagnetic fields computations near fold caustics—Part I, J. Comput. Appl. Math. 156 (2003) 93–125.

[4] R. Dautray, J.L. Lions, Mathematical Analysis and Numerical Methods for Science and Technology, Vol. 6, Springer, Berlin, 1993.

[5] B. Després, F. Lagoutière, J. Sci. Comput. 16 (4) (2001) 479–524.

[6] J.J. Duistermaat, Oscillatory integrals, lagrange immersions and unfolding of singularities, Comm. Pure Appl. Math. 27 (1974) 207–281.
[7] M.V. Fedoryuk, Partial Differential Equations, Springer, Berlin, 1988 (Chapter 1).
[8] W.L. Kruer, The Physics of Laser Plasma Interactions, Laser Plasma Interaction, Addison-Wesley, New York, 1988.
[9] O. Lafitte, I. Solliec, in preparation.
[10] D. Ludwig, Uniform asymptotic expansions at a caustic, Comm. Pure Appl. Math. 19 (1966) 215–250.
[11] I. Solliec, Optique géométrique eulerienne et calcul d'énergie électromagnétique en présence de caustiques de type pli, Ph.D. dissertation, Université Pierre et Marie Curie.